AN ABSTRACT OF THE THESIS OF

Pin Zhao for the degree of Master of Science in Materials Science through the Department of Electrical & Computer Engineering presented on January 14, 1994.

Title: Characterization and Applications of Low-Temperature-Grown MBE Gallium Arsenide.

Abstract approved: Redacted for privacy

Thomas K. Plant

Low-temperature (LT) MBE-grown GaAs material has recently been used for fast response, low dark current photodetectors. The material contains a high concentration of As precipitates which appear to act as spherical Schottky barriers with overlapping depletion regions making the GaAs semi-insulating. In this work, the electrical and optical characteristics of LT-GaAs are studied in *p-i-n* diodes, MSM photoconductors, and a new modulation-doped photoconductor using LT-GaAs grown at 225 °C, 300 °C, and 350 °C. The goal of this work was to measure the transport properties of LT-GaAs to resolve an ambiguity in the literature. Direct Hall mobility measurements proved unreliable due to high resistivity even in photoexcited samples. From the I-V behavior of *p-i-n* diodes, an estimate of carrier lifetime ranging from 4 ps to 130 ps for growth temperatures from 225 °C to 350 °C was made. MSM photoconductors fabricated on the LT-GaAs showed sub-nanosecond response and no evidence of the long tail always found in MSM photodetectors on semi-insulating GaAs. The new modulation-doped LT-GaAs photoconductor shows a gain of 300, a mobility of 500 cm^2 / Vs, and a response to wavelengths longer than 1500 nm. There appears to be both a transient, trap-related transport mechanism and a steady-state, recombination-related transport mechanism with significantly different properties.

Characterization and Applications of Low-Temperature-Grown MBE Gallium Arsenide

by

Pin Zhao

A THESIS

submitted to

Oregon State University

in partial fulfillment of

the requirements for the

degree of

Master of Science

Completed January 14, 1994

Commencement June 1994

APPROVED:

Redacted for privacy

Professor of Electrical and Computer Engineering in charge of major

Redacted for privacy

Head of Department of Electrical and Computer Engineering

Redacted for privacy

Director, Center for Advanced Materials Research

Redacted for privacy

Dean of Graduate School

Date thesis is presented January 14, 1994

Typed by Pin Zhao

Acknowledgment

I would like to express sincere gratitude to my advisor, Professor Thomas K. Plant, for his support, guidance, patience and many helpful suggestions throughout this work. Special thanks to Dr. S Subramanian for his assistance in device fabrication, experiment design and numerous discussions; Dr. Leon Uniger for the timely and high quality MBE sample growth.

I would also like to thank Dr. John F. Wager, Dr. S. Subramanian, and Dr. Gary Klinkhammer for serving on my graduate committee and providing useful suggestions.

My special thanks also goes to my parents for their continued support, advice and encouragement.

For my parents

Table of Contents

List of Figures

List of Tables

Characterization and Applications of Low-Temperature-Grown MBE Gallium Arsenide

1. Introduction

Gallium arsenide is a group III-V semiconductor. It has higher electron mobility, shorter carrier lifetime, and larger energy bandgap than other semiconductor materials such as silicon and germanium. These properties make it an ideal candidate for high-frequency, high-temperature, and radiation-resistant device applications. The basic properties of bulk GaAs are listed below in Table 1.1 [1].

Atoms/cm^3	4.42×10^{22}	Electron Mobility	8500cm^2/V-sec
Atomic Weight	144.63	Hole Mobility	400 cm^2/V-sec
Density	5.32 g/cm^3	Breakdown Field	~4×10^5 V/cm
Lattice Constant	5.6533 Å	n_i(300K)	~1.79×10^6/cm^3
Melting Point	1238 °C	Intrinsic Resistivity	~10^8 Ω-cm
Thermal Conductivity	0.46W/cm-°C	Band Gap (Direct)	1.424 eV
λ_g	0.87 μm	Dielectric Constant	13.1

Table 1.1 Properties of Bulk GaAs at 300 K.

GaAs has a zincblende structure in which the coordination is tetrahedral; that is, each atom, Ga or As, is symmetrically surrounded by four atoms of the other element, each located at the corners of a regular tetrahedron. The GaAs crystal lattice contains a repeating face-centered-cubic (f.c.c.) Ga sublattice atom of cube-edge length a=5.6533 Å interpenetrating a similar f.c.c. As sublattice of identical cube-edge length. The As sublattice is displaced by a vector $(\frac{a}{4},\frac{a}{4},\frac{a}{4})$ with respect to the Ga

sublattice origin (0, 0, 0). At room temperature and atmospheric pressure, the distance between nearest-neighbor Ga-As pairs is 2.45 Å.

Several types of structural imperfections can occur in the GaAs crystal lattice, including Ga and As vacancies (V_{Ga} and V_{As}), Ga and As interstitials (Ga_i and As_i), antisite substitutions — As on a Ga site (As_{Ga}) or Ga on an As site (Ga_{As}), and impurity substitutions on either site. These defects can affect the physical and electronic properties of GaAs, including diffusion, dislocation density, luminescence, carrier transport, recombination, and conductivity.

Recently a new type of GaAs epilayer has attracted the attention of researchers interested in semiconductor devices. The GaAs is grown by molecular beam epitaxy (MBE) on a GaAs substrate whose temperature is somewhere between 200 °C and 400 °C, well below the normal growth temperature of 575-600 °C for high quality GaAs. When annealed for 10 minutes at about 600 °C, the material (hereafter called LT-GaAs) is crystalline but nonstoichiometric with an approximately 1-1.5 at. % excess of As which is thought to exist in the form of cluster precipitates and/or point defects with a density of at least $10^{18}/cm^3$ [2,3]. The LT-GaAs is semi-insulating and the recombination time of photo-injected carriers can be as short as 300 fs [4], presumably related to the high arsenic defect/cluster concentration. It also has a wide sub-bandgap absorption due to deep defects [5]. The semi-insulating nature, sub-picosecond carrier lifetime, and sub-bandgap absorption make LT-GaAs an attractive material for ultrafast, laser activated high voltage switches and infrared photodetectors [6,7].

Photodetectors fabricated using GaAs are important in high speed optical-fiber communication systems operating in the near-infrared region (0.75 to 0.87 μm). They demodulate optical signals, that is, convert the optical variations into electrical variations, that are subsequently amplified and further processed. For such

applications the photodetectors must satisfy stringent requirements such as high sensitivity at operating wavelengths, high response speed, and minimum noise. In addition, the photodetector should be compact in size, use low biasing voltages, and be reliable under a wide range of operating conditions.

Most commercial optical receivers today are hybrid circuits of silicon-based electronics with Ge- or GaInAsP-based photonics, designed to detect the common fiber-optic long distance communication system wavelengths of 1.3 and 1.55μm. A preferred configuration would involve integrated electronic and photonic devices fabricated from one material, or from lattice-matched heterostructures such as InP/InGaAsP and InP/InAlAsP. Progress in the commercial development of InP-based integrated receivers, however, has been slow. And while high-performance GaAs-based integrated electronic circuits and receivers can now be fabricated reliably, conventional GaAs detectors are not sensitive in the 1.3-1.55 μm range. With the help of LT-GaAs, an all-GaAs 1.3 μm optical receiver chip should now be possible.

The aim of the research described in this thesis was to characterize LT-GaAs material grown in the MBE facility of the Department of Electrical and Computer Engineering, Oregon State University and to fabricate and test *p-i-n* diodes, metal-semiconductor-metal photoconductors (MSMPC), and metal-semiconductor-metal modulation-doped photoconductors (MODPC) made from this material. The research objectives were to gain a better understanding of the mechanism responsible for the reported sub-bandgap photoresponse and to measure the carrier lifetimes and mobilities as a function of growth temperature to be better able to model these devices and improve their performance.

2. Background

2.1 Low-temperature Grown GaAs

A new semi-insulating (SI) GaAs buffer material inserted between the active layer and the substrate was first developed by Smith *et al.* [8]. It was grown by MBE using Ga and As_4 beam fluxes, under arsenic-stable growth conditions, at a growth rate of 1 μm/h and at a substrate temperature of 200 °C. The new buffer layer material was crystalline, highly resistive, and optically inactive. A number of performance improvements for metal-semiconductor field-effect transistors (MESFET) fabricated in active layers on this buffer have been measured. Most significantly, backgating is eliminated, not merely reduced.

Kaminska *et al.* [9] performed a detailed transmission electron microscopy (TEM) investigation of cross-sectional samples of LT-GaAs and showed a high degree of crystal perfection. By X-ray diffraction and electron paramagnetic resonance (EPR) measurements on unannealed samples grown at 200 °C, they detected the largest lattice parameter of 5.660 Å and the highest concentration of arsenic antisite defects of 5×10^{18} / cm^3 ever observed for GaAs. After annealing at 600 °C for 10 minutes, the lattice parameter returned to that of GaAs grown at normal growth temperatures of approximately 600 °C, and the antisite defect concentration reduced to below the detection limit of 10^{18} cm^{-3}.

In 1989, Kaminska *et al.* [2] continued their TEM studies and confirmed a large arsenic-rich deviation stoichiometry (~1-1.5 at. %) for LT-GaAs MBE layers. X-ray rocking curves showed an isotropic lattice expansion of the 200 °C LT-GaAs annealed layer with a relative lattice parameter difference of $\Delta a/a_0 \approx 0.001$. Hall effect and EPR measurements revealed the presence of an acceptor level for LT-GaAs layers

at an energy of about 0.3 eV above the valence band, which might be due to gallium vacancies.

Warren *et al.* [3] observed the excess arsenic as hexagonal phase arsenic. Properties of the annealed low temperature buffer layer (LTBL) were explained by a simple model in which the arsenic precipitates act as buried Schottky barriers with "spherical" depletion regions. The layers become semi-insulating when either the doping level is low enough or the precipitate density is high enough for the depletion regions to overlap.

Gupta *et al.* [10] demonstrated that MBE-grown GaAs exhibits a sub-picosecond (<0.4 ps) carrier lifetime for growth temperature near 200 °C and annealed at 600 °C for 10 minutes. They found that annealed LT-GaAs is an ideal photoconductive material for the generation of sub-picosecond electrical pulses and for sub-picosecond sampling gates in guided-wave and terahertz-beam systems.

Van Driel *et al.* [11] obtained photoluminescence spectra from LT-GaAs and observed carrier distributions with a significant energy width. For the thermal distributions found under high excitation conditions, their results show that the carriers are very hot during their short lifetime. LT-GaAs with even shorter carrier lifetime may yield nonthermal distributions for carriers during the pulse, or thermal distributions with higher temperatures. In LT-GaAs, the high carrier temperature for short wavelength excitation, and/or the associated occupation of the L valley under transient excitation, probably accounts in part for the observed low carrier mobility. Better photodetector performance can probably be achieved with longer wavelength excitation for which more electrons will occupy the Γ valley at a lower temperature, resulting in a higher mobility.

Zhou *et al.* [12] used time-resolved luminescence to measure hot carrier dynamics in LT-GaAs grown at 200 °C. The radiative recombination coefficient is

comparable to that in GaAs and both electron and hole trapping times have been determined to be on the order of 1 ps. At high excitation, the energy loss rate of hot carriers is found to be more strongly reduced than in regular GaAs because of the enhanced role of hot phonon effects. The arsenic clusters and/or point defects also lead to higher initial carrier temperatures.

2.2 LT-GaAs Applications

Smith *et al.* [6] fabricated a photoconductive detector using LT-GaAs grown by MBE at a temperature of 200 °C. Autocorrelation measurements of the detector yielded a system limited response of ~7.5 ps. Electro-optic sampling was used to measure a temporal response of ~1.6 ps FWHM and an amplitude of ~0.4 V for a 10 V bias. These results compare favorably to the best results for any photoconductive switch yet reported.

Motet *et al.* [13] reported on the application of LT-GaAs for photoconductive switching using a pulse bias technique leading to the generation of an 825 V pulse with 1.4 ps rise time and duration of 4.0 ps. This represents the highest voltage ever obtained on the single picosecond time scale. This new capability to produce ultrashort high peak power electrical pulses is of interest for applications in fields such as nonlinear millimeter-wave spectroscopy, radar, high-energy physics, and ultrafast instrumentation.

Warren *et al.* [14] reported on the first LT-GaAs-based *p-i-n* photodiodes which operate in the 1.3 μm range. The devices exhibit low leakage currents at 295 K. Initial results from laterally-coupled devices have produced a factor of 10 increase in responsivity over the top-illuminated device with further improvement expected through optimization. The photoresponse speed in these devices is in excess of their initial testing limit of 50-100 GHz.

Interdigitated MSM photodiodes on LT-GaAs grown at 200 °C were fabricated by Klingenstein *et al.* [7]. These diodes have been compared to similar detectors produced on bulk intrinsic or SI GaAs. LT-GaAs diodes have a faster response (3.3 ps FWHM) and a lower-long-decay time tail but a smaller sensitivity compared to diodes on regular GaAs (6 ps FWHM). They have shown that mainly the displacement current contributes to the diode signal in the LT-GaAs diodes in accordance with the fact that the carrier trapping times are shorter than the carrier transit times in these structures. Compared to a simple stripline photodetector, the interdigitated diode structure offers the advantage of a significantly lower-bias voltage. Their experiments demonstrate that 4-6 V are sufficient to achieve a sensitivity of 85 mV/pJ instead of 80 V needed in a stripline.

Photoemission spectroscopy was performed by McInturff *et al.* [15] on two *p-i-n* structures with annealed LT-GaAs and unannealed LT-GaAs forming the device active layers. Annealed LT-GaAs was formed by low-temperature growth of GaAs at 225 °C, followed by an anneal at 600 °C for 30 minutes. The photoresponse was taken over the wavelength range 1.1 μm < λ < 1.6 μm. The annealed LT-GaAs device had a photoresponse similar to that measured by external photoemission of conventional metal-GaAs Schottky barriers. This result suggests that the sensitivity of this material to sub-bandgap light is due to internal Schottky barriers formed by arsenic precipitates embedded in a GaAs matrix. This result further suggests the possibility of enhanced sensitivity to 1.3 μm light and extended sensitivity to 1.5 μm light by embedding arsenic clusters in an alloy with a smaller band gap such as InGaAs.

3. Theory

In this chapter, the current-voltage characteristics of *p-i-n* and metal-semiconductor-metal (MSM) photodiodes are discussed. An electrical technique for determining the lifetime of a *p-i-n* photodiode is introduced.

3.1 *p-i-n* Photodiode

3.1.1 General Considerations

Under normal operating conditions, a junction photodiode is simply a reverse-biased *p-n* diode with a depletion region at the junction. This depletion region is characterized by a high electric field which allows photo-generated electron-hole pairs to separate and drift to a collection contact. The drift velocity in the intrinsic region is determined by the electric field and, in turn, by the mobility of the crystal. The electron-hole pairs which are photo-generated outside the depletion region begin to diffuse toward the depletion region and either recombine or are swept away upon entering the depletion region. The speed of response of a photodetector is determined by the drift time in the depletion region, the diffusion time outside the depletion region, the capacitance of the depletion region, and, in some circumstances, the contact resistance. Photo-response and quantum efficiency are determined in large part by the width, W, of the depletion region. A larger depletion region absorbs more incident light which translates to a higher quantum efficiency. Also, as the depletion width increases, device capacitance decreases, enhancing device response time under load-limited circumstances. However, transit-time delay also increases with W, setting the device's fundamental speed limitation. Therefore, there is a trade-off between

quantum yield and speed of response under nonload-limited circumstances. To enhance the quantum efficiency of photodiodes, it is desirable to increase the depletion region width, W, in some way. This is done by growing an intrinsic material (doped at a much lower density than the junction materials) region between the n and p layers or by implanting or diffusing a compensating material into the host. This structure is known as a *p-i-n* diode. The schematic structure and the corresponding energy-band diagram for a *p-i-n* diode are shown in Figure 3.1.1 [1]. To make this a photodiode, a non-metalized region is left around or inside the p-type or n-type ohmic contact so light can enter through this p or n layer and into the wider intrinsic region.

The *p-i-n* photodiode is one of the most common photodetectors because the depletion-region thickness (the intrinsic layer) can be tailored to optimize the quantum efficiency and frequency response. Light absorption in the semiconductor produces hole-electron pairs. Pairs produced in the depletion region or within a diffusion length of it will eventually be separated by the electric field, leading to current flow in the external circuit as carriers drift across the depletion layer.

3.1.2 Quantum Efficiency and Responsivity

The quantum efficiency is the number of electron-hole pairs generated per incident photon:

$$\eta = (I_p / q) / (P_{opt} / h\nu), \tag{1}$$

where I_p is the photo-generated current by the absorption of incident optical power P_{opt} at a wavelength λ (corresponding to a photon energy $h\nu = h\frac{c}{\lambda}$).

The responsivity is the ratio of the photocurrent to the optical power:

$$\Re = \frac{I_p}{P_{opt}} = \frac{\eta q}{h\nu} = \frac{\eta\lambda(\mu\text{m})}{1.24} \quad \text{A/W} \tag{2}$$

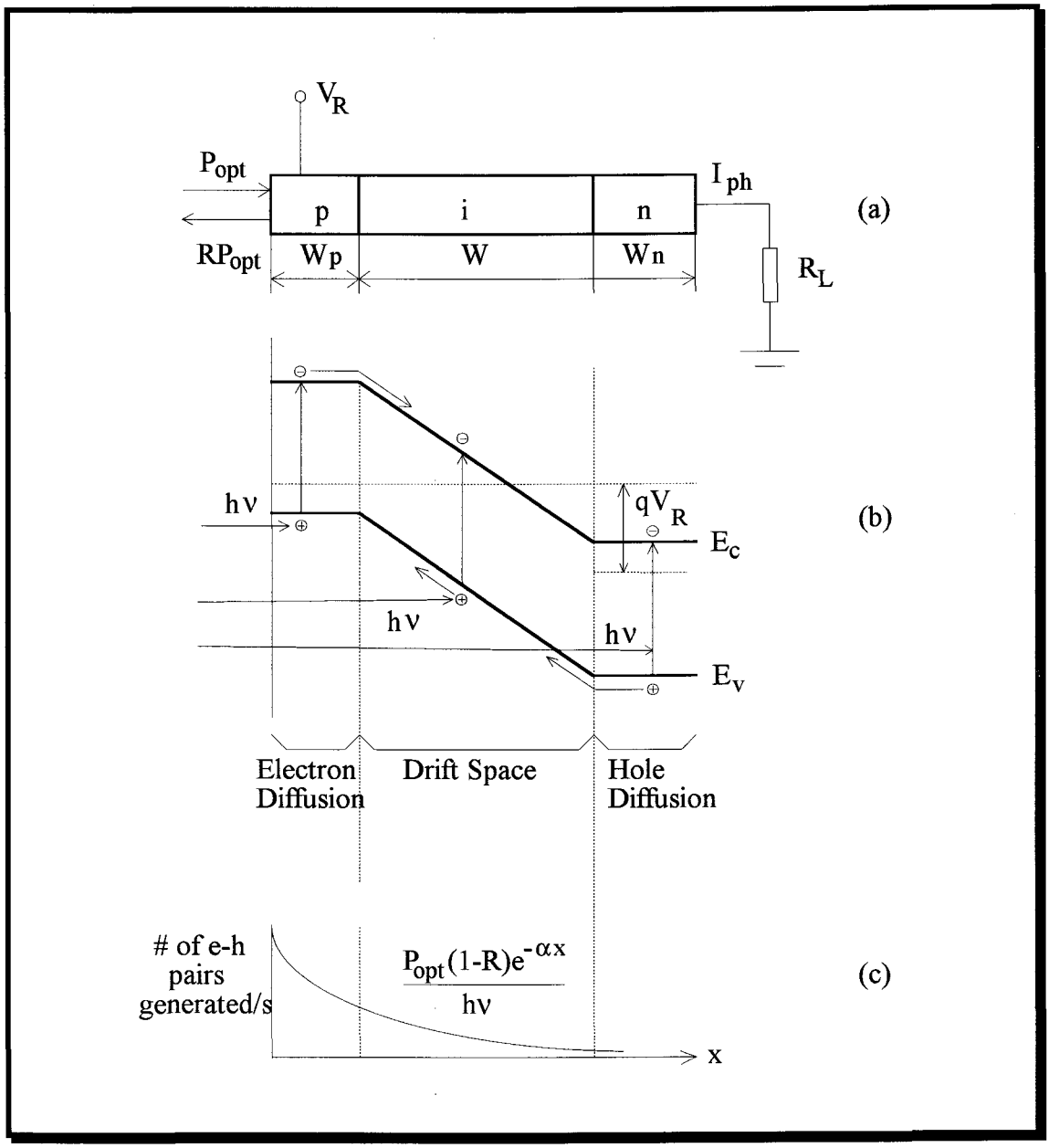

Figure 3.1.1 Operation of a *p-i-n* photodiode. (a) Cross-sectional view of *p-i-n* diode, (b) Energy-band diagram under reverse bias, (c) Carrier generation characteristics.

Therefore, for a given quantum efficiency, the responsivity increases linearly with wavelength. For an ideal photodiode (η=1), $\Re$=(λ/1.24)(A/W), where λ is expressed in microns.

3.1.3 Current Considerations

Under steady-state conditions the total current density through the reverse-biased depletion layer is given by

$$J_{tot} = J_{dr} + J_{diff} \tag{3}$$

where J_{dr} is the drift current due to carriers generated inside the depletion region and J_{diff} is the diffusion current density due to carriers generated outside the depletion region and diffusing into the reverse-biased junction. We shall now derive the total current under the assumptions that the thermal generation current can be neglected and that the surface p layer is much thinner than $1/\alpha$, where α is the absorption coefficient (in cm^{-1}). The hole-electron generation rate is given by

$$G(x) = \Phi_0 \alpha e^{-\alpha x} \tag{4}$$

where Φ_0 is the incident photon flux per unit area given by $P_{opt}(1-R)/Ah\nu$, where R is the reflection coefficient and A is the device area. The drift current density J_{dr} is thus given by

$$J_{dr} = -q\int_0^W G(x)dx = q\Phi_0(1-e^{-\alpha W}) \tag{5}$$

where W is the depletion-layer width. For $x > W$, the minority-carrier density (holes) in the bulk semiconductor is determined by the one-dimensional diffusion equation

$$D_p \frac{\partial^2 p_n}{\partial x^2} - \frac{p_n - p_{n0}}{\tau_p} + G(x) = 0 \tag{6}$$

where D_p is the diffusion coefficient for holes, τ_p is the lifetime of excess carriers, and

p_{n0} is the equilibrium hole density. The solution of Eq. (6) under the boundary conditions $p_n = p_{n0}$ for $x = \infty$ and $p_n = 0$ for $x = W$ is given by

$$p_n = p_{n0} - (p_{n0} + C_1 e^{-\alpha W}) e^{(W-x)/L_n} + C_1 e^{-\alpha x} \tag{7}$$

with $L_p = \sqrt{D_p \tau_p}$ and

$$C_1 \equiv (\frac{\Phi_0}{D_p}) \frac{\alpha L_p^2}{1 - \alpha^2 L_p^2} \tag{8}$$

The diffusion current density is given by $J_{diff} = -qD_p (\frac{\partial p_n}{\partial x})_{x=W}$,

$$J_{diff} = q\Phi_0 \frac{\alpha L_p}{1 + \alpha L_p} e^{-\alpha W} + q p_{n0} \frac{D_p}{L_p} \tag{9}$$

and the total current density is

$$J_{tot} = q\Phi_0 (1 - \frac{e^{-\alpha W}}{1 + \alpha L_p}) + q p_{n0} \frac{D_p}{L_p} \tag{10}$$

Under normal operating conditions, the term involving p_{n0} is much smaller than the first term so that the total photocurrent is proportional to the photon flux. The quantum efficiency can be obtained from Eqs. (1) and (10),

$$\eta = \frac{J_{tot}/q}{P_{opt}/Ah\nu} = (1 - R)(1 - \frac{e^{-\alpha W}}{1 + \alpha L_p}). \tag{11}$$

For high quantum efficiency, a low reflection coefficient with $\alpha W >> 1$ is desirable. However, for $W >> \frac{1}{\alpha}$, the transit-time delay may be considerable.

3.2 Metal-Semiconductor-Metal Photoconductor

3.2.1 General Considerations

The simplest form of a metal-semiconductor-metal (MSM) structure is a two terminal device having a uniformly doped semiconductor slice with metal contacts on opposite sides of the slice as shown in Figure 3.2.1(a) [16]. The energy band diagram for a symmetrical MSM structure at thermal equilibrium is shown in figure 3.2.1(b) where Φ_{n1} and Φ_{n2} are the barrier heights for the two contacts, V_{D1} and V_{D2} are the built-in potentials, respectively, and L is the thickness of the slice. If the areas of the contacts are equal and $\Phi_{n1} = \Phi_{n2}$, we have a symmetrical MSM structure.

It is clear that an MSM structure is basically two Schottky barriers connected back to back. Under an applied voltage, one of the contacts called contact No. 1 is reverse-biased and the other, called contact No. 2, is forward-biased. The charge distribution, electric field, and potential profile of an MSM structure under bias (with positive bias on contact 2) are shown in Figure 3.2.2. As the applied voltage increases, the sum of the two depletion widths also increases. Eventually, at the reach-through voltage, V_{RT}, the two depletion regions touch each other and the sum equals L. This situation is illustrated in Figure 3.2.3(a).

As the voltage increases further, a point is reached at which the electric field at $x = L$ becomes zero and the energy band at $x = L$ becomes flat. This is the flat-band voltage, V_{FB}, shown in Figure 3.2.3(b). The maximum voltage that can be applied to the MSM structure is limited by the punch-through breakdown near the maximum field at contact No. 1.

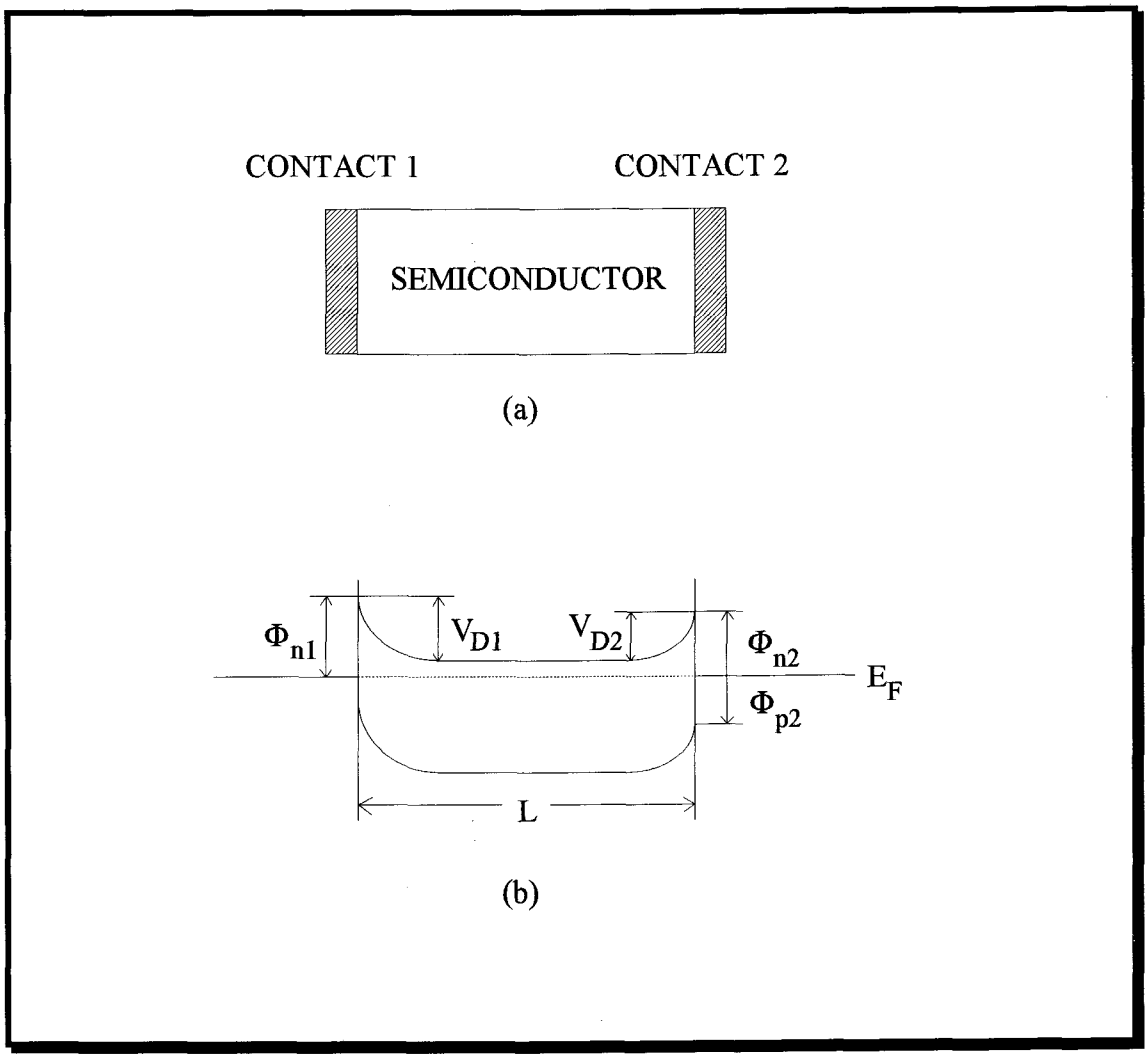

Figure 3.2.1 (a) Schematic diagram of an MSM structure, (b) The corresponding energy band diagram at thermal equilibrium.

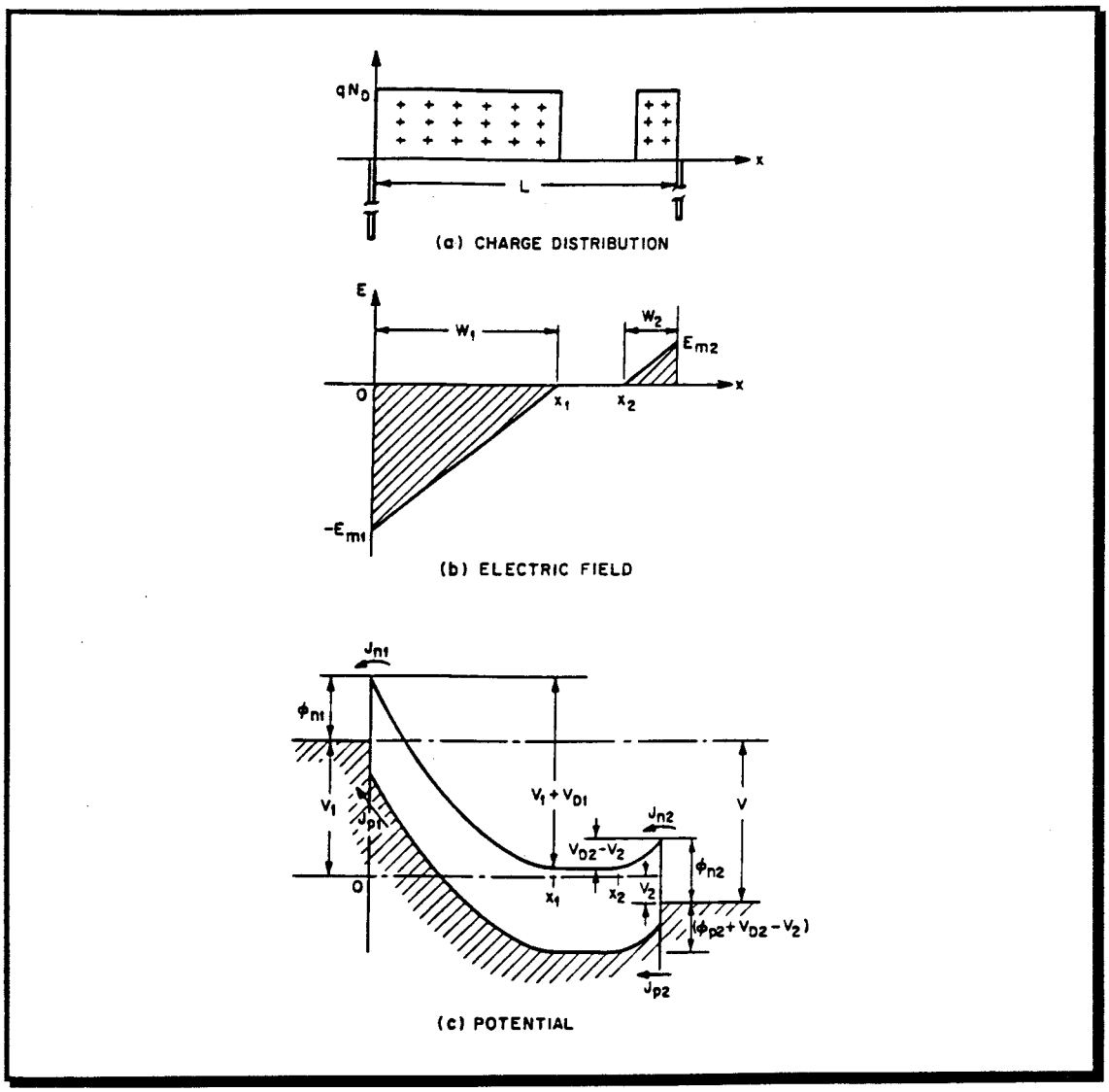

Figure 3.2.2 The charge distribution, electric field, and potential profile of an MSM structure under bias (with positive bias on contact 2).

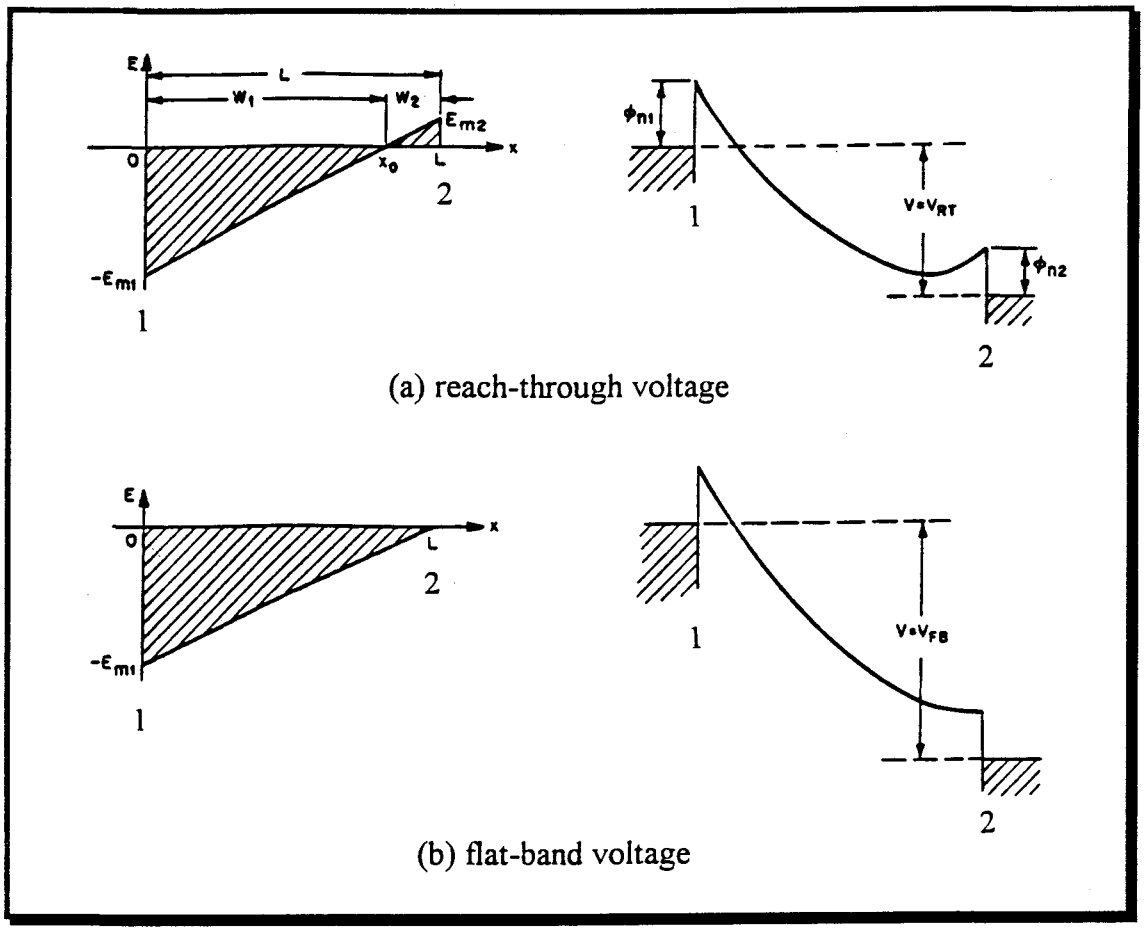

Figure 3.2.3 (a) Condition of reach-through at which the two depletion regions touch each other, (b) Condition of flat-band at which the energy band at x=L becomes flat.

3.2.2 Current-Voltage Characteristics

The total current is the sum of electron current and hole current. Following are the definitions of some important quantities:

J_{ns} = electron saturation current density $\equiv A_p^* T^2 e^{-q\Phi_{n1}/kT}$

where A_p^* is the effective Richardson constant for holes.

J_{ps} = hole saturation current density $\equiv A_p^* T^2 e^{-q\Phi_{p2}/kT}$

V_{FB} = flat-band voltage $\cong \frac{qNV_D L^2}{2\varepsilon_s} - (V_{D1} - V_{D2})$

V_{RT} = reach-through voltage $\cong V_{FB} - \sqrt{4V_{D1}V_{D2}}$

$\beta = \frac{q}{kT}$

Now the total current density can be expressed as follows under different applied bias conditions,

(a) Small voltage V<V_{RT}

$$J = J_{n1} + J_{p1}$$

$$= J_{ns} e^{\beta\Delta\Phi_{n1}} (1 - e^{-\beta V_1}) + \left[\frac{qD_p p_{n0} \tanh[(x_2 - x_1)/L_p]}{L_p} (1 - e^{-\beta V_1}) \right.$$

$$\left. + \frac{J_{ps} e^{-\beta V_{D2}}}{\cosh[(x_2 - x_1)/L_p]} (e^{\beta V_2} - 1) \right] \qquad (12)$$

(b) $V_{RT} < V < V_{FB}$

$$J = J_{ns} e^{\beta\Delta\Phi_{n1}} + J_{ps} \left[e^{-\frac{\beta(V - V_{FB})^2}{4(V_{FB} + \Delta V_D)}} - e^{-\beta V_{D2}} \right] \qquad (13)$$

(c) $V > V_{FB}$

$$J = J_{ns} e^{\beta\Delta\Phi_{n1}} + J_{ps} e^{\beta\Delta\Phi_{p2}} \qquad (14)$$

Up to now, the operation of both *p-i-n* and MSM photodiodes has been discussed in detail. Recently, Swaminathan *et al.* [17] found an electrical technique to determine the ambipolar lifetime in the *p-i-n* diode. This technique requires a careful forward I-V measurement and is discussed in the next section.

3.3 Determination of the Ambipolar Lifetime

The conventional diode equation is given by

$$I_F = I_s(\exp\frac{qV}{nkT} - 1), \tag{15}$$

where I_F is the forward current, I_s is the diode saturation current, q is the electronic charge, n is the ideality factor which varies from 1 to 2, k is Boltzmann's constant, V is the voltage-drop across the depletion regions, and T is the absolute temperature. Assuming a good ohmic contact, the applied voltage is the sum of the voltage-drop across the depletion regions and the i region, which can be expressed as,

$$V_a = V + V_i = V + I_F R_i. \tag{16}$$

where R_i is the resistance of the i region. Thus V can be expressed as

$$V = V_a - I_F R_i. \tag{17}$$

When the voltage-drop across the depletion regions is much larger than $\frac{2kT}{q} = 51.8$ mV, the exponential term in Eq. (15) is much greater than 1 and Eq. (15) becomes

$$I_F = I_s \exp\frac{q(V_a - I_F R_i)}{nkT}. \tag{18}$$

Differentiating Eq. (18), we get

$$R_i = \frac{dV_a}{dI_F} - \frac{nkT}{qI_F}. \tag{19}$$

According to Eq. (19), a R_i versus $\frac{1}{I_F}$ curve can be plotted from $\frac{dV_a}{dI_F}$ and $\frac{1}{I_F}$ data as obtained from an I-V curve.

Under dc forward bias

$$R_i = \frac{V_i}{I_F} = \frac{\rho_i l}{A}, \tag{20}$$

where ρ_i is the resistivity of the i region, l is the thickness of the i region, and A is the diode area. The resistivity of the i region can be written as

$$\rho_i = \frac{1}{nq\mu_n + pq\mu_p}, \tag{21}$$

where n and p are the electron and hole concentrations and μ_n and μ_p are the electron and hole mobilities in the i region. Substituting Eq. (21) into Eq. (20), we get

$$R_i = \frac{kT}{q^2}\frac{2b}{(1+b)^2}\frac{l}{D_a An}, \tag{22}$$

where $b = \mu_n / \mu_p$ and D_a is the ambipolar diffusion constant. In deriving Eq. (22) we have made use of the Einstein relation $D = \frac{kT}{q}\mu$ and the relation $D_a = \frac{2D_p b}{1+b}$.

The diode current due to recombination can also be expressed as

$$I_F = \frac{AnqL_a}{\tau_a} + nqSL_sP, \tag{23}$$

where L_a is the ambipolar diffusion length, τ_a is the excess carrier (ambipolar) lifetime, P is the diode perimeter length, S is the surface recombination velocity, and L_s is the surface diffusion length . The first term in Eq. (23) is the bulk recombination current and the second term is the surface recombination current. Substituting for n from Eq. (23) in Eq. (22) gives

$$R_i = \frac{kT}{q}\frac{2b}{(1+b)^2}\frac{l}{D_a A}\frac{(\frac{L_a A}{\tau_a} + SL_s P)}{I_F}, \tag{24}$$

Eq. (24) indicates that the resistance of the *i* region is inversely proportional to the forward current. From Eq. (20), the slope of the R_i vs. $\frac{1}{I_F}$ curve is the voltage-drop across the *i* region.

From Eqs. (20) and (24), we can get

$$V_i = \frac{kT}{q}\frac{2b}{(1+b)^2}\frac{l}{D_a}\left(\frac{L_a}{\tau_a} + \frac{SL_s P}{A}\right). \tag{25}$$

Increasing the forward current tends to increase V_i ohmically but it also increases the injected carrier density leading to a decrease in V_i with the net result of V_i being unaffected. Thus knowing D_a, b, (SL_s), and V_i obtained from the slope of R_s vs. $\frac{1}{I_F}$ curve, the carrier lifetime τ_a can be calculated.

4. Experimental Procedure

This chapter describes the experimental procedures used in this research. It includes the sample growth, device fabrication, electrical and optical measurements of the *p-i-n* diode, the MSM photoconductor (MSMPC), and the modulation-doped photoconductor (MODPC).

4.1 Sample Growth and Device Fabrication

Three types of devices were fabricated: *p-i-n* diodes, interdigitated MSM photoconductors, and interdigitated modulation-doped photoconductors. The *p-i-n* diode materials were grown by MBE with *i* layer growth temperatures of 225 °C, 300 °C, and 350 °C, respectively. The MSMPC was fabricated on the semi-insulating (SI) LT-GaAs layer grown at 300 °C. The MODPC was fabricated using 300 °C LT-GaAs as the channel layer. The fabrication procedure involves photolithography and thermal evaporation of gold, titanium, and zinc. This section describes these processes in detail.

4.1.1 *p-i-n* Diode Fabrication

Semiconductor layers used in this study were grown by MBE at a rate of 1 μm / h. The substrate used for epitaxial layer growth for the *p-i-n* diode structure was <100> oriented n-type GaAs (Si: 5×10^{18} / cm^3). A cross-sectional view of the structure grown is shown in Figure 4.1.1.

Beginning with the clean n^+ GaAs substrate, a 0.25 μm thick $10^{18}/cm^3$ Si-doped GaAs buffer layer was first grown at a substrate temperature of 600 °C. The

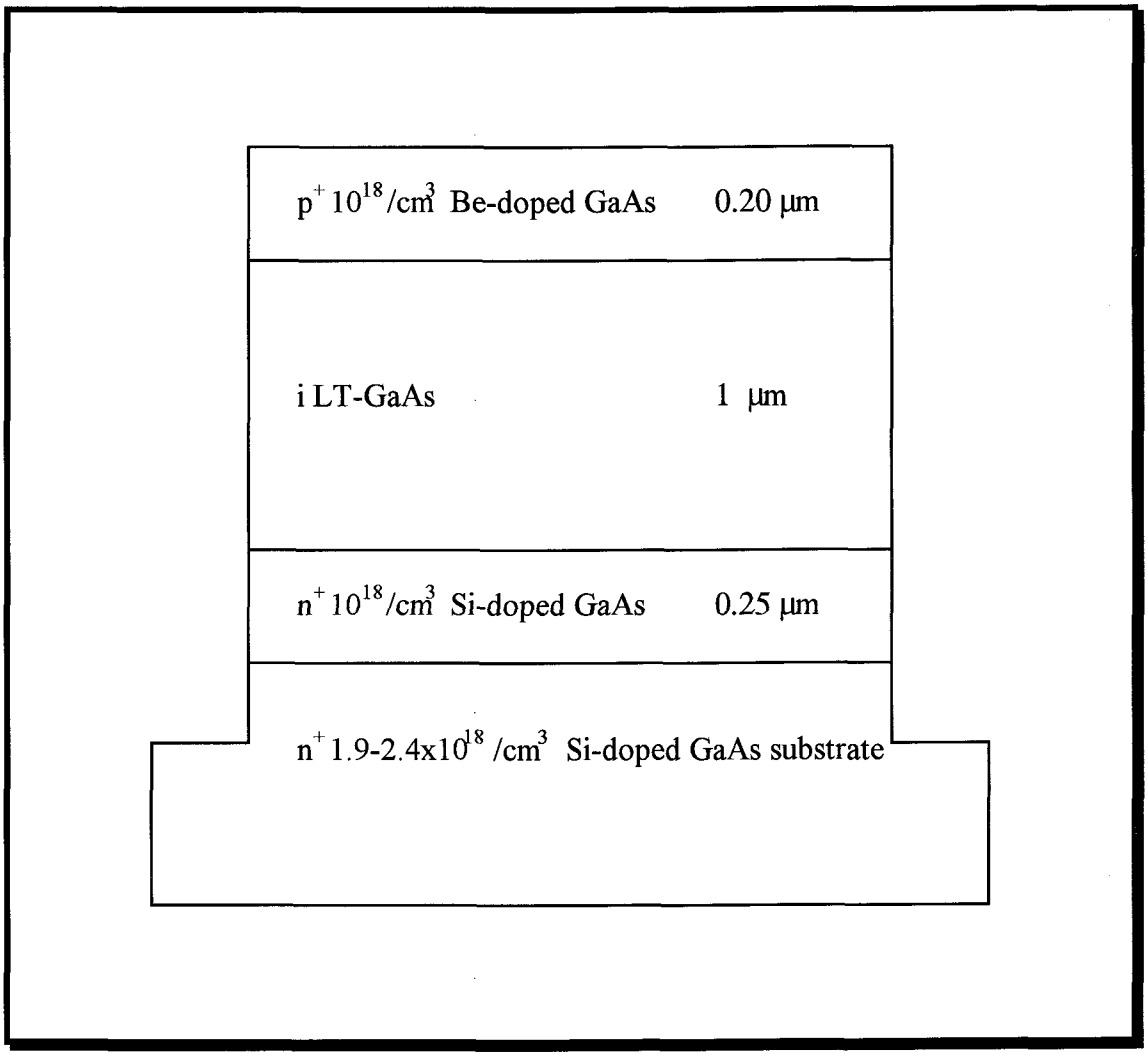

Figure 4.1.1 Epitaxial structure of MBE-grown *p-i-n* diode.

substrate temperature was then reduced for the growth of an intrinsic LT-GaAs layer. Three samples were grown in this research with 1 μm thick intrinsic LT-GaAs layers grown at 225 °C, 300 °C, and 350 °C, respectively. Finally, the substrate temperature was then raised to 575 °C and a 0.2 μm $10^{18}/cm^3$ Be-doped p-GaAs cap layer was grown. The 12 minutes required to grow this cap layer provided an in-situ anneal of the LT-GaAs layer at 575 °C.

A 1 cm × 1 cm piece was cleaved from the full quarter of a 2" wafer to conserve material. Since a full *p-i-n* photodiode mask set was not available, we used a one-mask process using the mask shown in Figure 4.1.2(a) with 200, 400 and 800 μm diameter dots to fabricate mesa-etched *p-i-n* diodes. The final *p-i-n* devices were metalized with *p*-ohmic metal (AuZnAu) completely over the top of the mesa so light can only enter the junction region around the edges of the mesa. This makes them virtually unusable as photodiodes but nevertheless useful for electrical testing to assess transport properties of LT-GaAs. The devices were finally passivated with Na_2S to reduce surface leakage currents around the mesas [18]. The *p-i-n* processing steps are listed in detail in Appendix A.

4.1.2 Metal-Semiconductor-Metal Photoconductor Fabrication

The substrate used for the MSM structure epitaxial layer growth was <100> oriented undoped, semi-insulating (SI) GaAs. First the substrate temperature was set to 300 °C and a 2 μm thick undoped LT-GaAs layer was grown at a growth rate of 1 μm/h. Then the substrate temperature was raised to 575°C and a 200 Å thick, $10^{18}/cm^3$ Si-doped GaAs cap layer was grown for protection. A cross-sectional diagram of the MSM epitaxial structure is shown in Figure 4.1.3.

Again, a 1 cm × 1 cm piece was cleaved from the MBE-grown semiconductor material. In contrast to the *p-i-n* diode processing procedure, the MSM

photoconductors were processed by a lift-off procedure for the Schottky contacts. The 200 μm × 200 μm active area MSM photoconductors use a one-mask lift-off process with the mask shown in Figure 4.1.2(b). Following exposure of the negative photoresist, a 5 minute soak in chlorobenzene was used to harden the surface to give an overhanging "lip" after developing. The 1200 Å Au Schottky contacts were evaporated and lifted off with the photoresist, leaving the interdigitated MSM photoconductor pattern behind. The Schottky contacts were not annealed. The MSM processing steps are listed in detail in Appendix B.

Another MSM photoconductor was made on a piece of *p-i-n* (with a 1 μm thick *i* layer grown at 225 °C) structure material by completely wet etching the top *p* layer off before depositing the MSM electrodes. The processing steps were the same as mentioned before.

4.1.3 Modulation-doped Photoconductor Fabrication

The substrate used for the modulation-doped photoconductor structure epitaxial layer growth was <100> oriented undoped, SI GaAs. First, the substrate temperature during growth was set to 580 °C, a 0.5 μm thick intrinsic GaAs buffer layer was first grown. The substrate temperature was then reduced to 300 °C and a 0.5 μm thick intrinsic LT-GaAs layer was grown. Next, the substrate temperature was raised to 580 °C and a 100 Å thick intrinsic $Al_{0.2}Ga_{0.8}As$ layer was grown. Then a 350 Å thick n-type $Al_{0.2}Ga_{0.8}As$ layer (Si: $10^{18}/cm^3$) was grown at the same substrate temperature. Finally a 100 Å thick GaAs cap layer with $10^{18}/cm^3$ Si-doping was grown without changing the substrate temperature. A cross-sectional view of the structure is shown in Figure 4.1.4.

A 1 cm × 1 cm piece was cleaved from the MBE-grown semiconductor material. Similarly to the MSM photoconductor processing 1200 Å Au/Ge/Ni ohmic

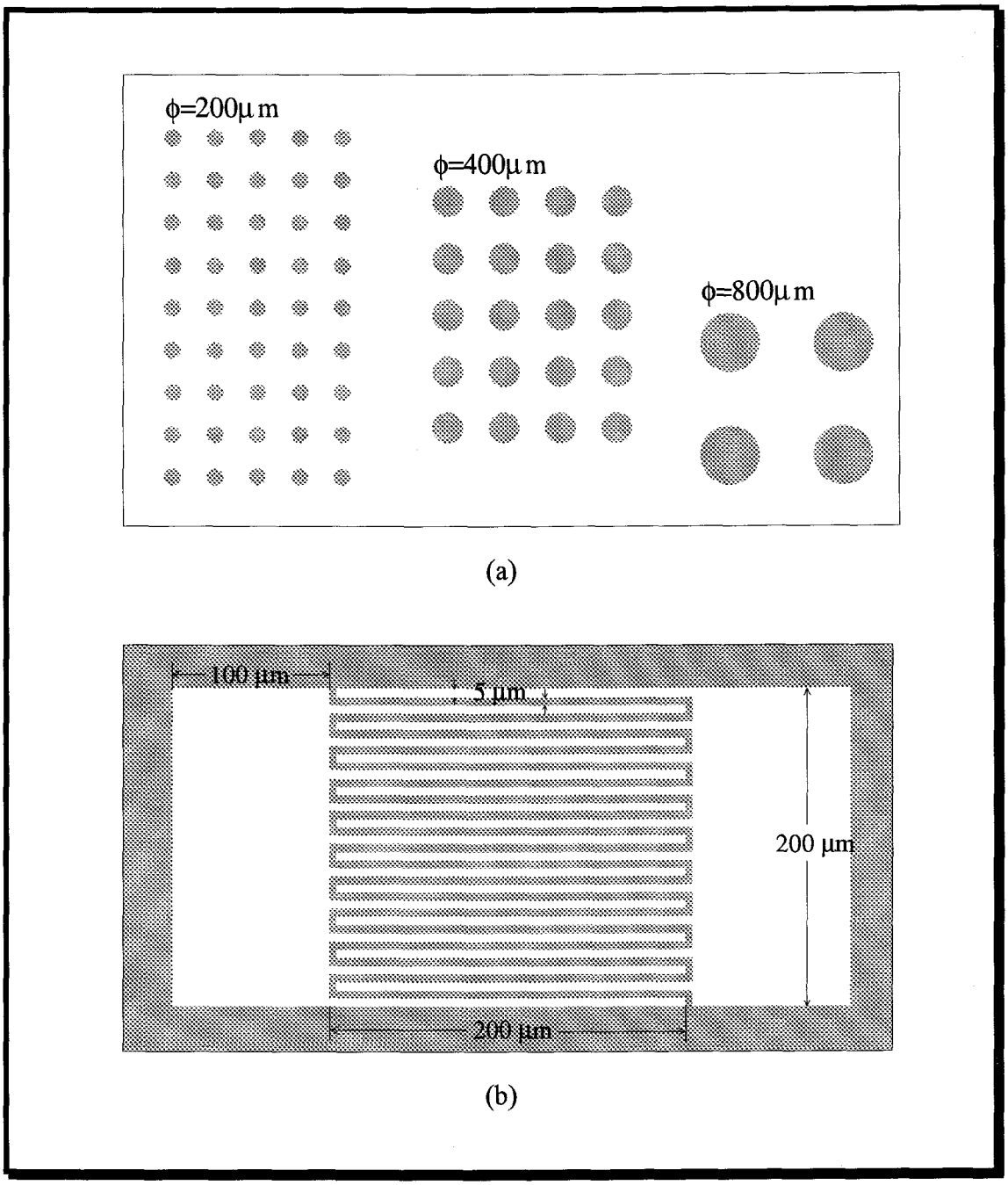

Figure 4.1.2 Mask (a) three different diameter *p-i-n* dot mask, (b) MSM interdigitated structure mask.

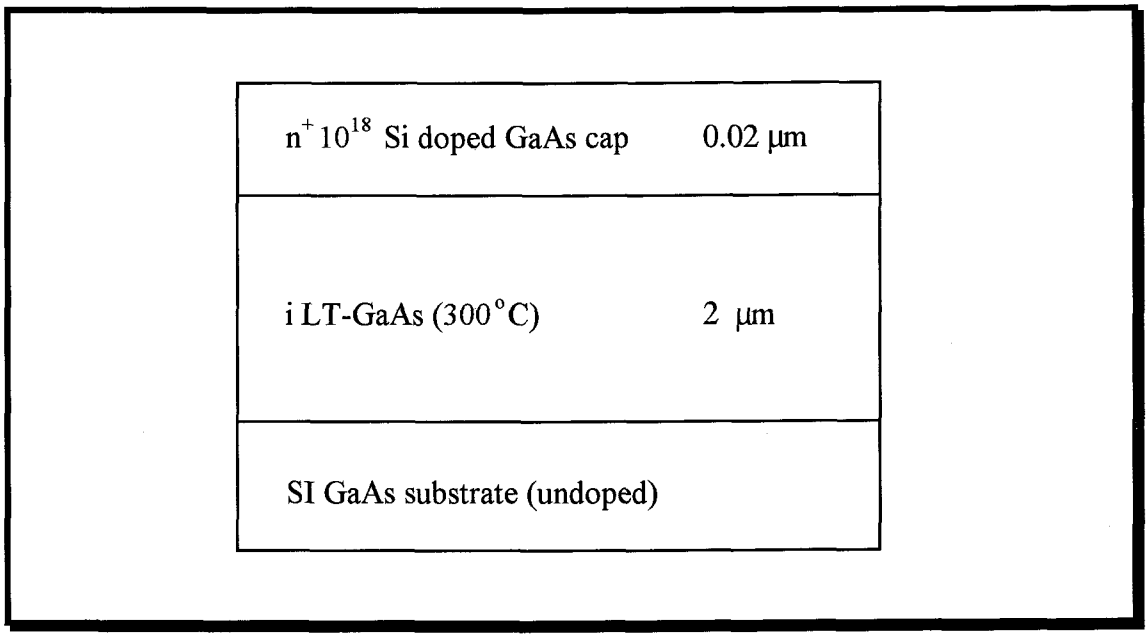

Figure 4.1.3 Epitaxial structure of MBE-grown MSM photoconductor material.

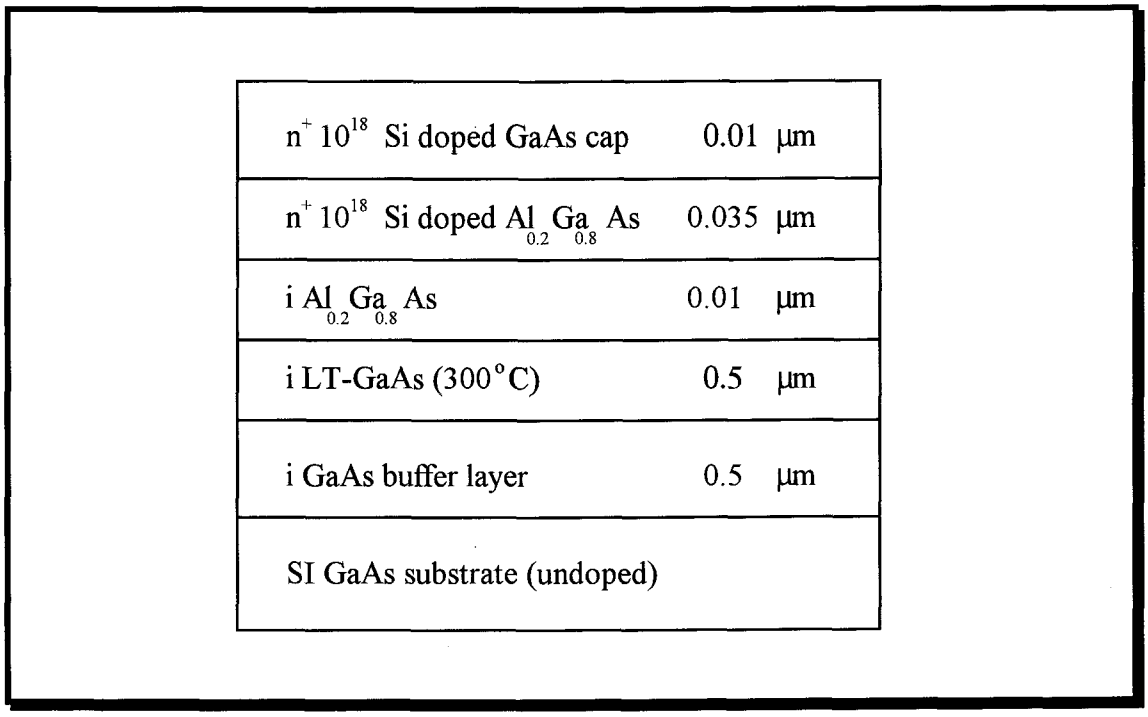

Figure 4.1.4 Epitaxial structure of MBE-grown modulation-doped photoconductor material.

contacts were evaporated and lifted off with the photoresist, leaving the interdigitated pattern behind. The ohmic contacts were then annealed at 500 °C for 3 minutes.

4.2 Device testing

4.2.1 I-V Characterization of the Devices

After the processing of the devices, they were all electrically tested using a microprobe station and a Hewlett-Packard 4145B parameter analyzer. The *p-i-n* diodes were tested in the dark, the MSMPC's were tested both in the dark and under He-Ne laser excitation, and the MODPC's were tested both in the dark and under microscope light excitation.

4.2.2 Spectral and Temporal Response Measurements

4.2.2.1 Spectral Response Measurement of the MSMPC's and the MODPC's

One possible advantage of LT-GaAs detectors is their reported sub-bandgap photoresponse at 1.3 μm and 1.55 μm [14]. In order to study the spectral properties of the LT-GaAs material, a simple spectral transmission measurement was performed using the experimental setup shown in Figure 4.2.1. Two samples were prepared for the measurement. One was a commercial semi-insulating GaAs substrate. The other was the same substrate material with a 2 μm layer of LT-GaAs grown at 300 °C on one surface. The back sides of both samples were optically polished to prevent scattering. An automobile quartz-halogen headlight lamp driven at 12 V and 4.8 A (P=58 W) provided a bright black-body source. A germanium *p-i-n* photodiode,

reverse biased at 1.5 V, was used to detect the transmitted light. Its working wavelength range was 0.8 μm - 1.8 μm. The light source was mechanically chopped at 200 Hz and the signals were amplified by a lock-in amplifier. The experimental data were sent to a computer for data processing.

A 2 mm × 2 mm piece of the MSM material made on SI LT-GaAs containing 4 MSM interdigitated photoconductors was then mounted into a ceramic DIP package with silver epoxy. An individual photoconductor was wire bonded with 1 mil gold wire to two of the package leads and connected in series outside the package with a 15 kΩ load resistor. A 20 V bias voltage was applied across the photoconductor and load resistor, and a spectral photoresponse measurement was performed. The experimental setup, shown in Figure 4.2.2, is similar to that in Figure 4.2.1. The germanium *p-i-n* photodiode was again used to calibrate the light source. After the calibration of the light source the normalized photoresponse of the MSM photoconductor was obtained.

A modulation-doped photoconductor sample was similarly mounted into a ceramic DIP package. By using a small microprobe station and connecting in series with a 15 kΩ load resistor, the spectral response measurements were performed under different bias voltages.

4.2.2.2 Temporal Response Measurement of the MSMPC

In order to measure the picosecond carrier lifetime of the LT-GaAs, another cleaved MSM sample made on SI LT-GaAs was connected onto a 50 Ω transmission line with gold-wire bond to measure the photoresponse of the MSM photoconductor. The schematic diagram of the transmission line is shown in Figure 4.2.3. The dc end was connected to the bias power supply, and the ac end was connected to a 500 MHz Tektronix 7904 oscilloscope with a 26 ps rise time sampling unit for measurement.

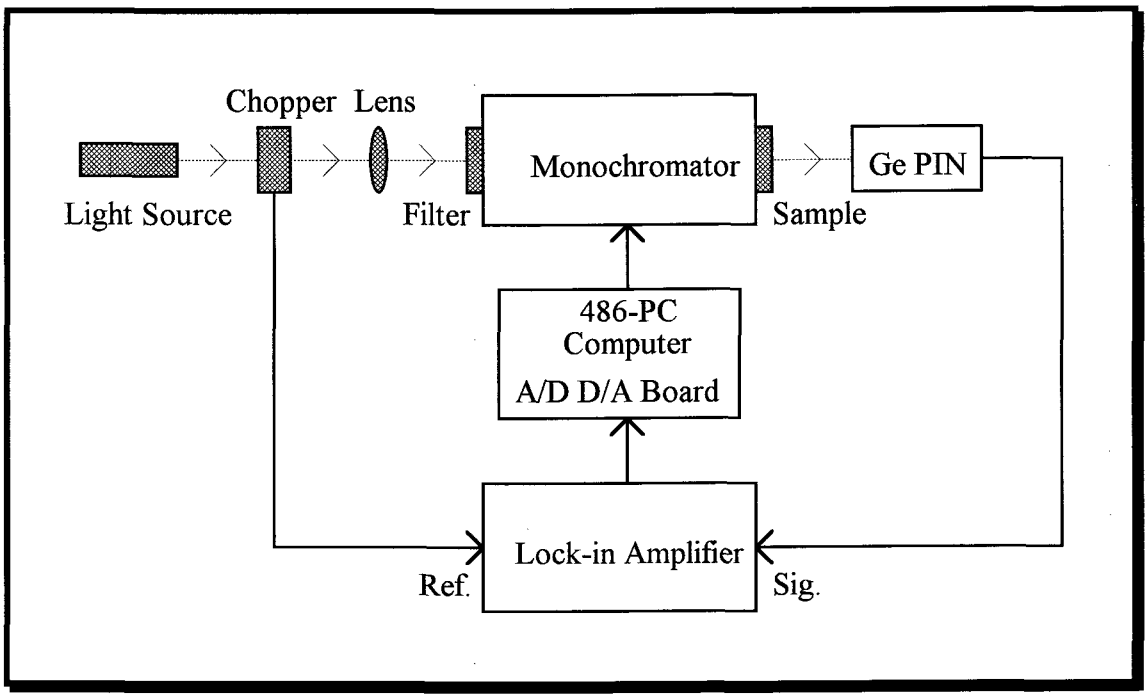

Figure 4.2.1 Experimental setup to measure the transmission spectrum of the MSM LT-GaAs layer.

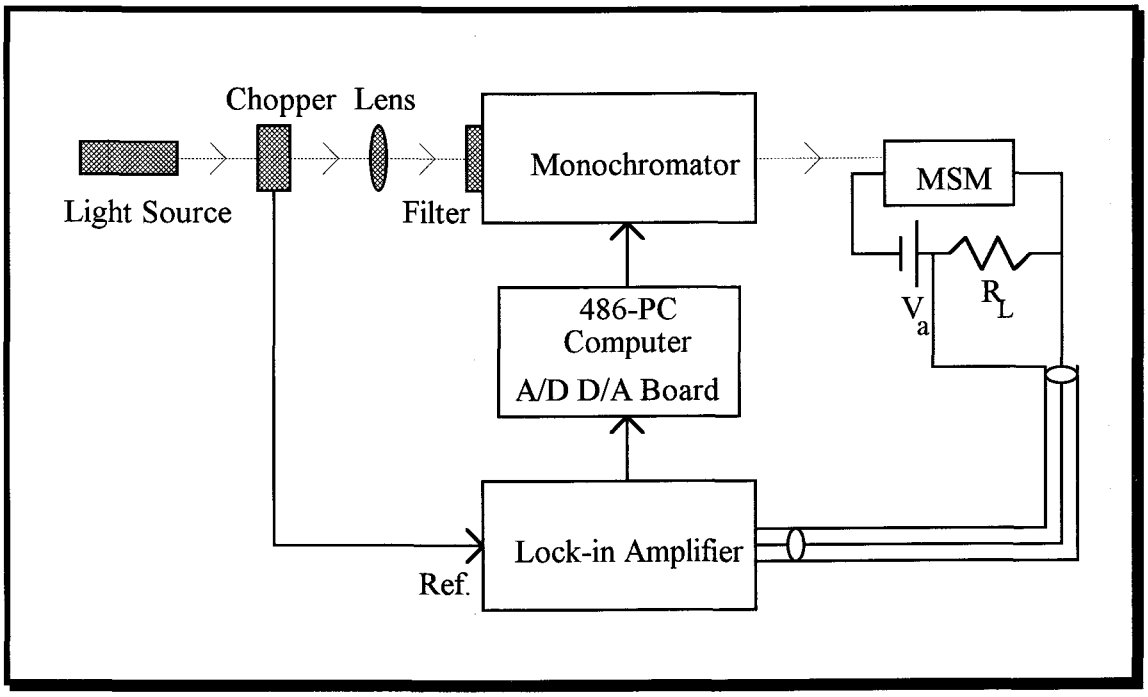

Figure 4.2.2 MSM photoconductor spectral response measurement setup.

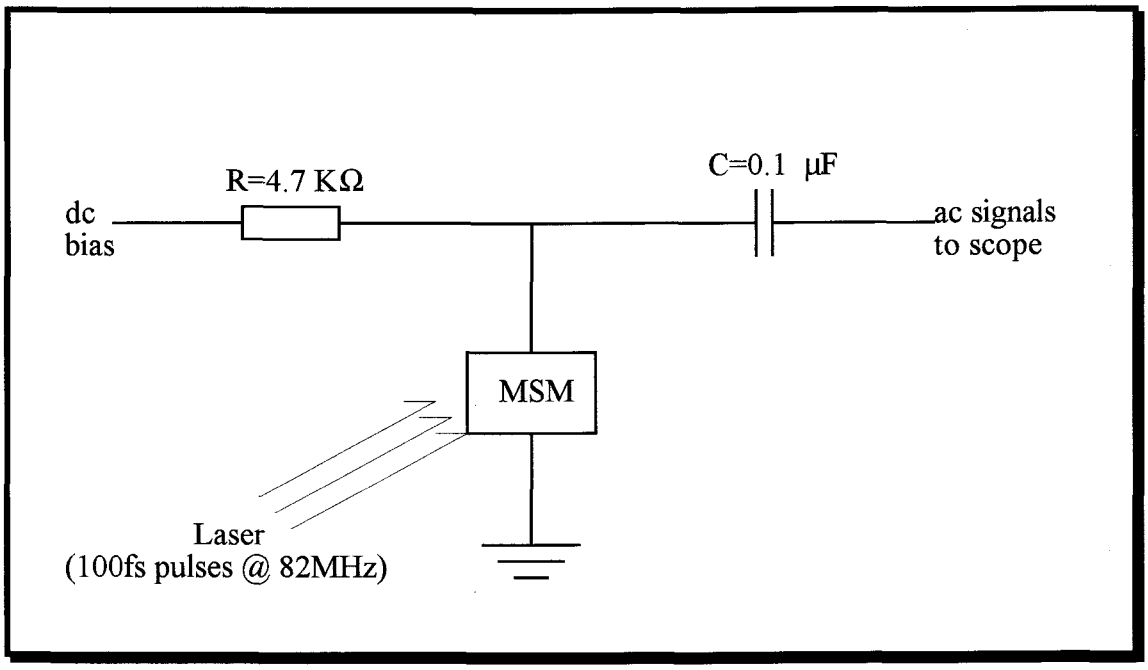

Figure 4.2.3 Schematic diagram of the transmission line photoconductor mount and laser excitation source.

The optical pulses with λ=830 nm and 100 fs duration were derived from an 82 MHz repetition rate mode-locked Ti:sapphire laser with an average output power of 300 mW. With 15 volt bias, the optical signals were detected by the MSM photoconductor. This experiment was done in the Physics Department at University of Oregon in cooperation with Prof. M. G. Raymer.

The MSM sample made on *p-i-n* structure material (with the *i* layer grown at 225 °C and the *p* layer removed) was also connected into a 50 Ω package and a temporal response measurement was made, to compare the speed of the 300 °C photoconductor.

5. Experimental Results and Discussion

5.1 Carrier Lifetime Determination in the LT-GaAs

The "forward" $\log(I_F)$-V characterization curves of the *p-i-n* diodes with *i* layers grown at 225 °C, 300 °C, and 350 °C are shown in Figures 5.1.1, 5.1.2, and 5.1.3, respectively. Each figure shows data for 200 μm, 400 μm, and 800 μm diameter diodes which were processed together on the same sample to assure uniformity. On each figure is also shown a logarithmically linear region corresponding to an ideality factor of n=2. The forward current should be mainly dominated by recombination current due to the high resistivity of the *i* layer. Because both *p* and *n* layers are much more heavily-doped than the *i* layer, any injection of carriers from *p* and *n* layers into the *i* layer can be regarded as high-level injection. Under both recombination and high-level injection conditions, the forward current has a theoretical ideality factor of n=2. Each figure shows parts of the curves with such a linear slope; however the 350 °C annealed curves are less consistent. For larger bias voltages, the forward current begins to saturate because of series resistance.

The forward $\log(I_F)$-V curves of the same diameter photodiodes grown at three different temperatures are shown in Figures 5.1.4, 5.1.5, and 5.1.6 for the three diameters 200 μm, 400 μm, and 800 μm, respectively. They all show that as the growth temperature of the *i* layer decreases, the voltage required to achieve the same amount of current increases. The resistance of the *i* layer increases because more excess arsenic precipitates are introduced during growth [9]. These excess arsenic precipitates act as buried Schottky barriers with spherical depletion regions [3]. As the arsenic precipitate concentration increases, the volume of the depleted GaAs increases and, hence, the resistivity of the LT-GaAs increases. Further increasing of

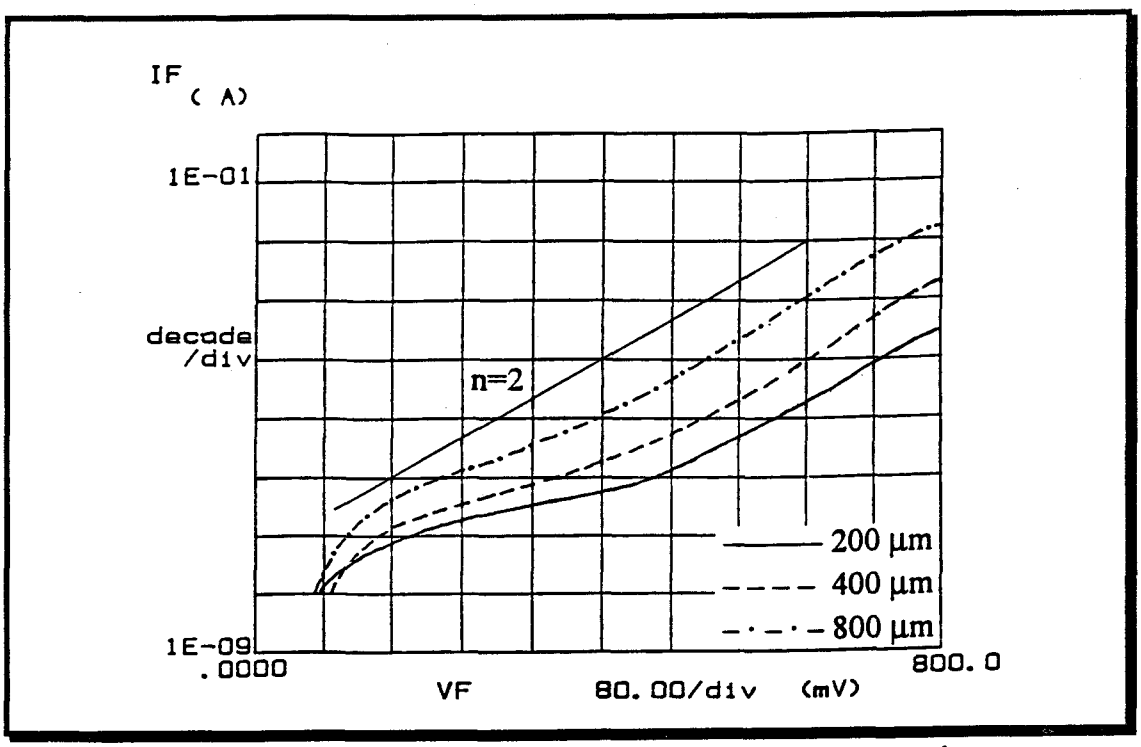

Figure 5.1.1 log(I)-V characterization curves of the *p-i-n* diodes with the *i* layer grown at 225 °C.

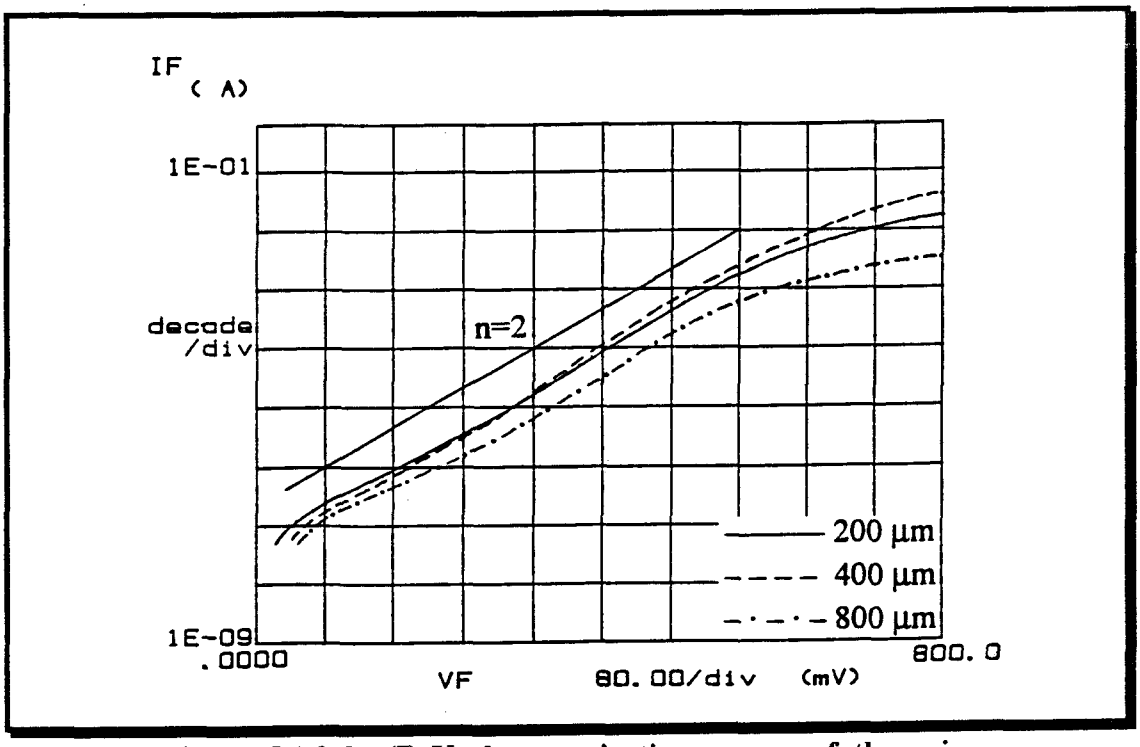

Figure 5.1.2 log(I)-V characterization curves of the *p-i-n* diodes with the *i* layer grown at 300 °C.

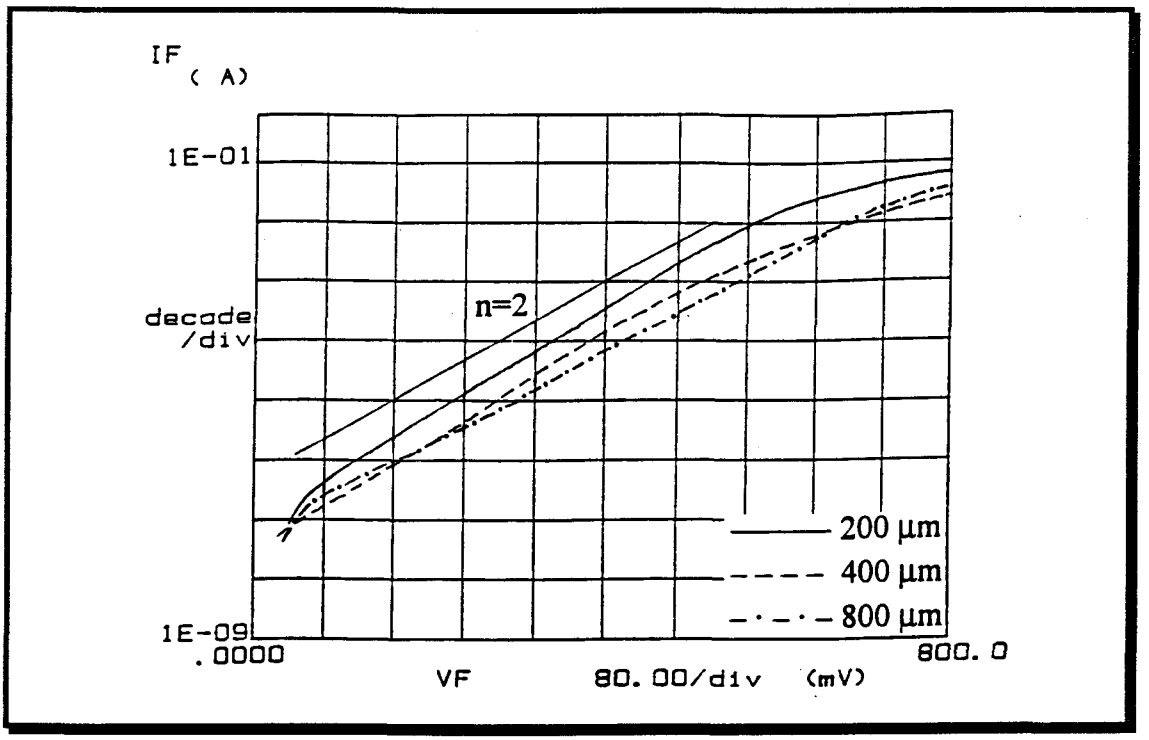

Figure 5.1.3 log(I)-V characterization curves of the *p-i-n* diodes with the *i* layer grown at 350 °C.

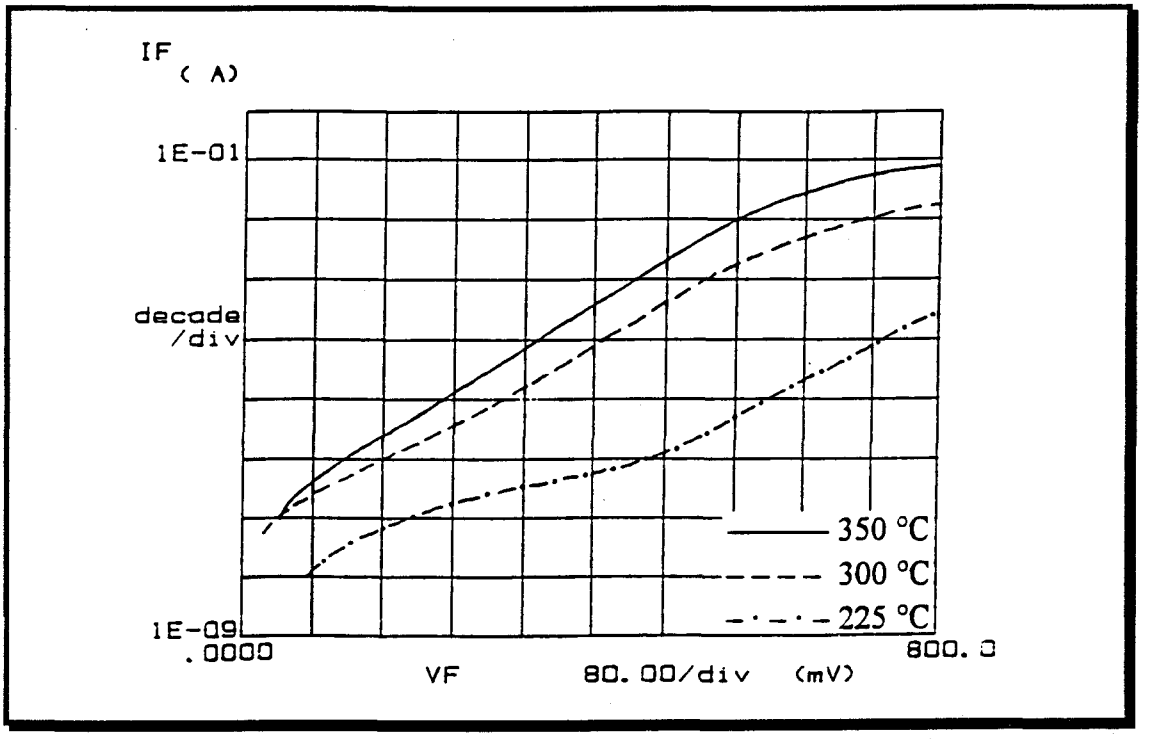

Figure 5.1.4 log(I)-V characterization curves of the 200 µm *p-i-n* diodes with the *i* layer grown at 225 °C, 300 °C, and 350 °C.

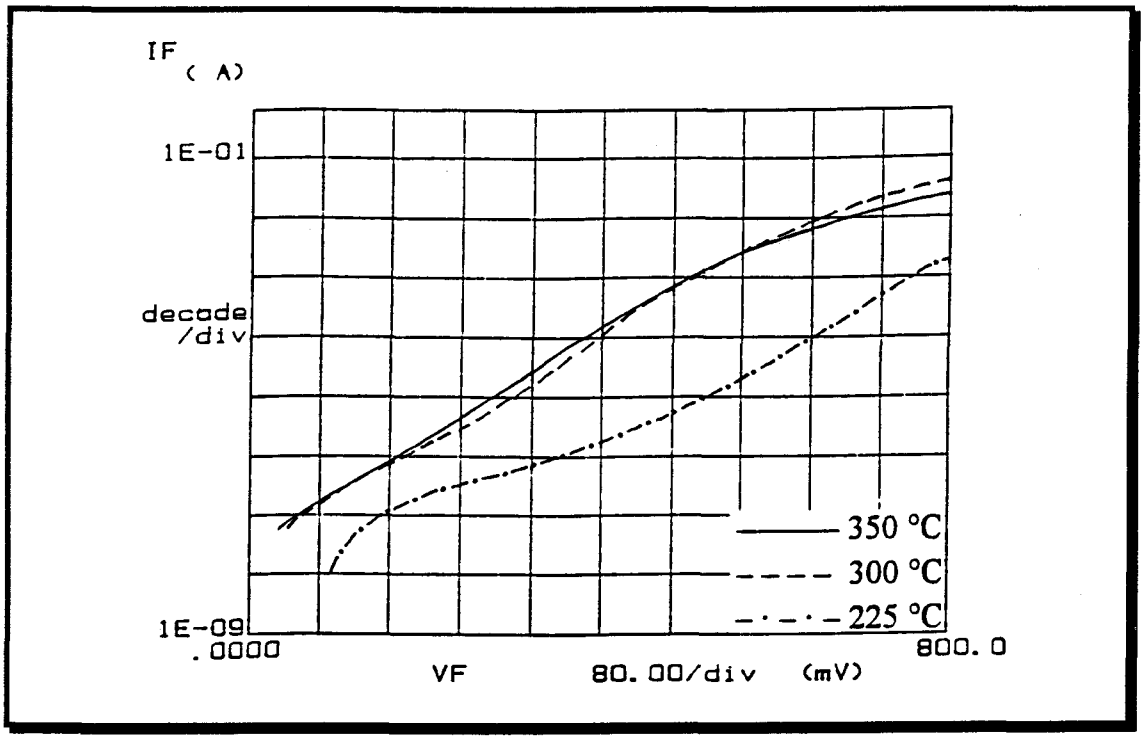

Figure 5.1.5 log(I)-V characterization curves of the 400 μm *p-i-n* diodes with the *i* layer grown at 225 °C, 300 °C, and 350 °C.

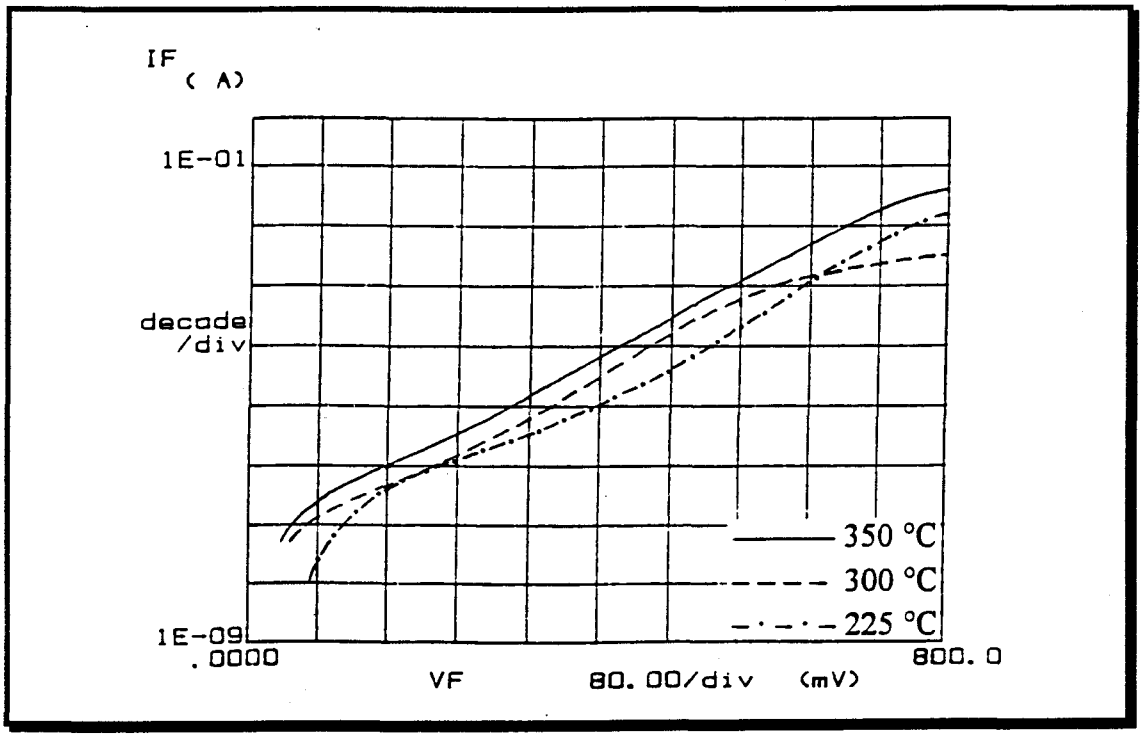

Figure 5.1.6 log(I)-V characterization curves of the 800 μm *p-i-n* diodes with the *i* layer grown at 225 °C, 300 °C, and 350 °C.

the arsenic precipitate concentration causes the overlap of the spherical depletion regions and the material becomes semi-insulating.

In the n=2 region, the $\frac{dV_a}{dI_F}$ and $\frac{1}{I_F}$ data were taken from the I-V curves and the resistance of the *i* region R_i was calculated using Eq. (19) in section 3.3,

$$R_i = \frac{dV_a}{dI_F} - \frac{nkT}{qI_F}. \tag{1}$$

The R_i versus $\frac{1}{I_F}$ curves were plotted in Figures 5.1.7, 5.1.8, and 5.1.9 for three different growth temperature, respectively. Figure 5.1.10 shows the R_i versus $\frac{1}{I_F}$ curve of one diameter for three growth temperatures. The voltage drop across the *i* layer is obtained from the slope of the curve (see section 3.3). The results are listed in Table 5.1.1 below.

Dot Diameter (μm)	V_i (mV) 225 °C	V_i (mV) 300 °C	V_i (mV) 350 °C
200	98.8	42.9	21.3
400	108.4	42.3	23.4
800	100.8	44.9	19.5
Average	102.7	43.4	21.4

Table 5.1.1 Voltage drop across the *i* layer grown at 225 °C, 300 °C, and 350 °C for three diameter *p-i-n* diodes.

Now the ambipolar lifetime theory can be applied. Recall Eq. (25) in Chapter 3, which is repeated below,

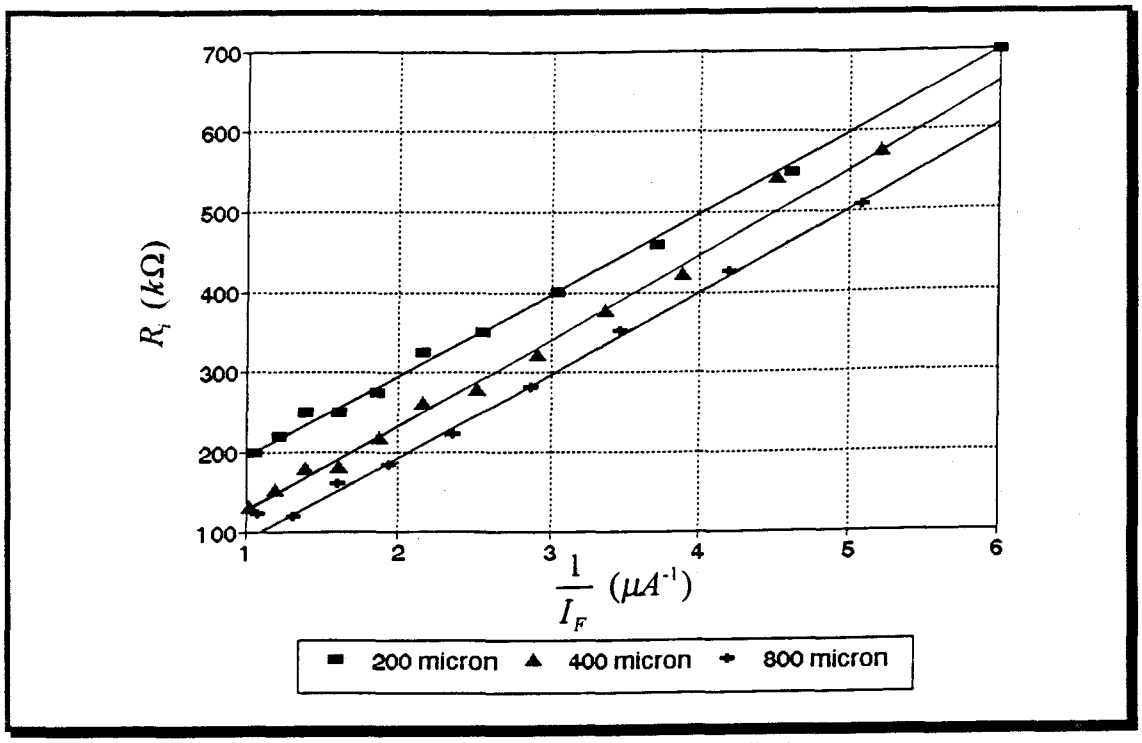

Figure 5.1.7 Intrinsic resistance of LT-GaAs grown at 225 °C versus inverse of forward current.

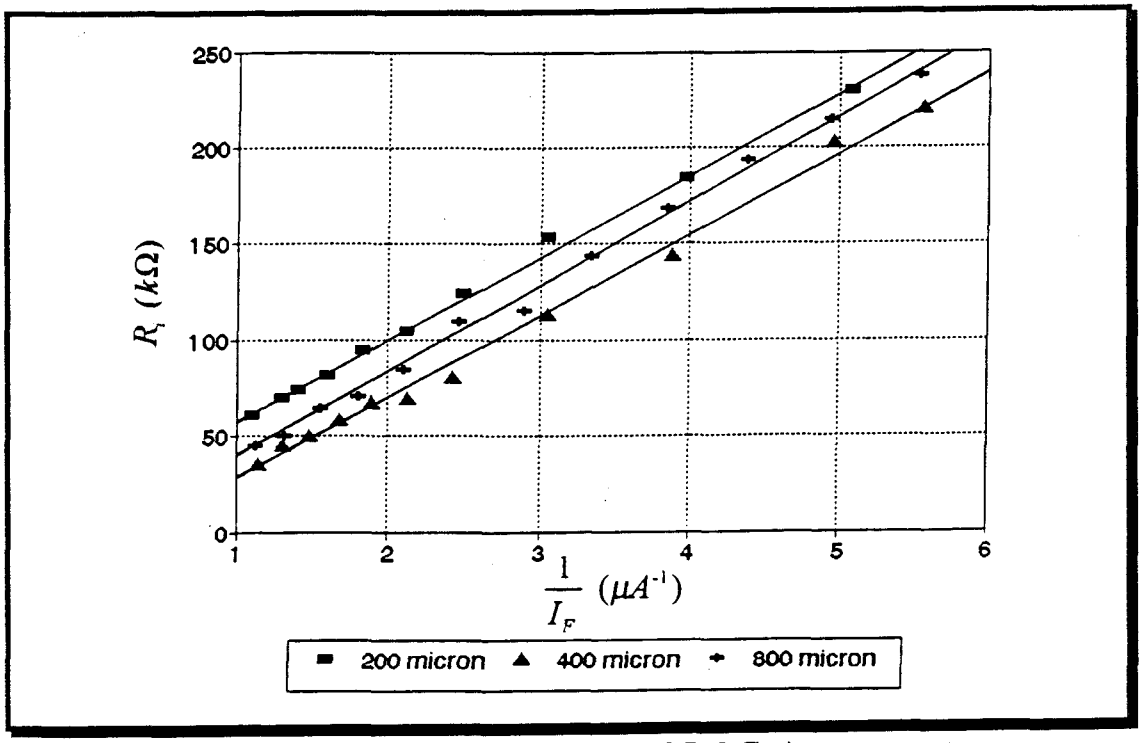

Figure 5.1.8 Intrinsic resistance of LT-GaAs grown at 300 °C versus inverse of forward current.

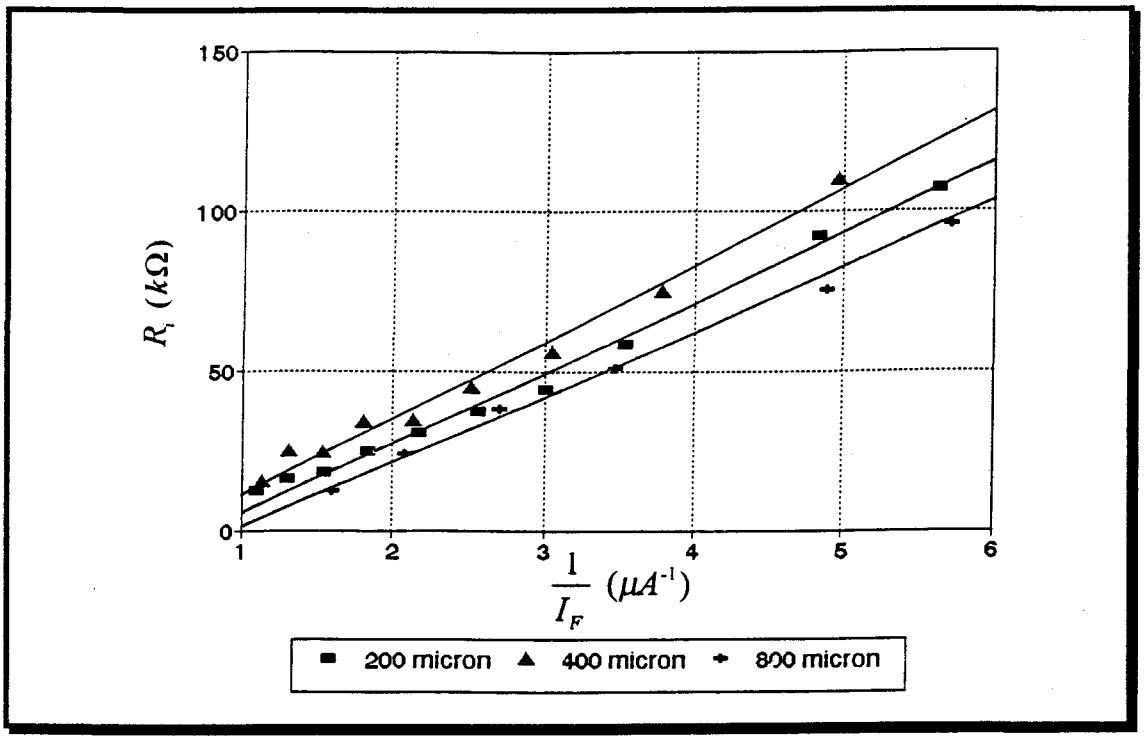

Figure 5.1.9 Intrinsic resistance of LT-GaAs grown at 350 °C versus inverse of forward current.

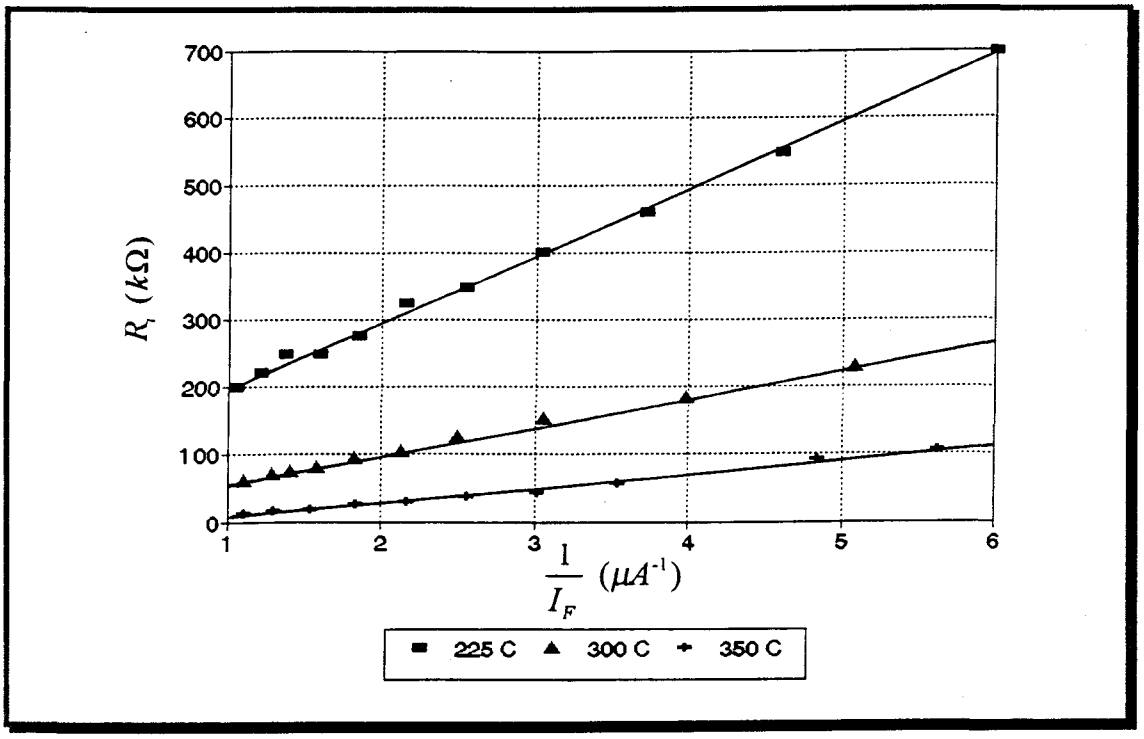

Figure 5.1.10 Intrinsic resistance of LT-GaAs of 200 μm diodes versus inverse of forward current.

$$V_i = \frac{kT}{q}\frac{2b}{(1+b)^2}\frac{l}{D_a}\left(\frac{L_a}{\tau_a}+\frac{SL_sP}{A}\right). \quad (2)$$

The first term in Eq. (2) is always much greater than the second term. Thus the second term can be neglected. Substituting the ambipolar diffusion length $L_a = \sqrt{D_a \tau_a}$ into Eq. (2), gives

$$V_i = \frac{kT}{q}\frac{2b}{(1+b)^2}\frac{l}{\sqrt{D_a \tau_a}}. \quad (3)$$

There are three unknown terms in Eq. (3): (1) the ratio of the electron mobility to the hole mobility b; (2) the ambipolar carrier lifetime, τ_a; and (3) the ambipolar diffusion length D_a. In nearly all semiconductors, b varies from 1 to 10. Smith [19] found that the Hall mobility at room temperature in annealed LT-GaAs is relatively high (~1000 cm^2 / Vs). Assuming an electron mobility of 1000 cm^2 / Vs and using values of V_i from Table 5.1.1, the carrier lifetime can be calculated. Table 5.1.2 lists the calculated carrier lifetime results for b values of 5 and 10.

b	τ_a @ 225 °C (ps)	τ_a @ 300 °C (ps)	τ_a @ 350 °C (ps)
5	5.7	31.8	130.9
10	3.7	20.7	85.0

Table 5.1.2 Calculated carrier lifetime for various *b* values with the carrier mobility of 1000 cm^2 / Vs.

Even though the lifetimes calculated in Table 5.1.2 are in agreement with the reported lifetimes measured by transient experiments [10], the 1000 cm^2 / Vs carrier mobility is not reasonable for a material containing a high concentration of defects. Gupta *et al.* [10] estimated the carrier mobility in LT-GaAs to be 120-150 cm^2 / Vs. Using a mobility of 100 cm^2 / Vs, the carrier lifetimes would be 10 times larger as listed in Table 5.1.3.

b	τ_a @ 225 °C (ps)	τ_a @ 300 °C (ps)	τ_a @ 350 °C (ps)
5	57	318	1309
10	37	207	850

Table 5.1.3 Calculated carrier lifetime for various *b* values with the carrier mobility of 100 cm^2 / Vs.

These last calculated lifetime values, assuming μ=100 cm^2 / Vs, are larger than the reported picosecond trapping times [12] or sub-picosecond lifetimes [10] which were derived from photoexcited short-pulse response measurements. The I-V measurement of the *p-i-n* diodes is a steady-state measurement associated mainly with the recombination of carriers while the transient measurement includes deep trapping processes [20]. The LT-GaAs contains As precipitates with a density on the order of $10^{17}/cm^3$. It has been shown in hydrogenated amorphous silicon that the recombination time is much longer than the deep trapping time in materials with large density of traps [21]. A similar phenomenon could be present here in the LT-GaAs due to the large concentration of As precipitates after annealing and many other crystal defects also, before annealing. Harmon *et al.* [22] observed that, after annealing, the measured carrier lifetime in LT-GaAs increased by more than an order of magnitude over that in unannealed material.

5.2 Absorption Spectrum Analysis of LT-GaAs

Reports of LT-GaAs having useful photoresponse to 1.3 μm and 1.5 μm signals make it important to examine the material absorption properties at sub-bandgap energies. The measured transmission spectrum of the SI GaAs substrate is shown in Figure 5.2.1(a). The transmitted intensity can be expressed as

$$I_{sub} = I_0 e^{-\alpha_{sub} x_{sub}} (1 - R_{sub})^2, \quad (4)$$

where I_0 is the incident light intensity, α_{sub} is the absorption coefficient of the GaAs substrate, x_{sub} is the thickness of the substrate, and R_{sub} is the reflection coefficient at the air/GaAs interface (~30%).

The measured transmission spectrum of a 2 μm layer of 300 °C LT-GaAs on a GaAs substrate is shown in Figure 5.2.1(b). The transmitted intensity can be expressed as

$$I_{LT+sub} = I_0 e^{-\alpha_{sub} x_{sub} - \alpha_{LT} x_{LT}} (1-R_{LT})(1-R_{sub}), \tag{5}$$

where α_{LT} is the absorption coefficient of the LT-GaAs, x_{LT} is the thickness of the LT-GaAs, and R_{LT} is the reflection coefficient at the air/LT-GaAs interface.

Both the LT-GaAs and the GaAs substrate should have nearly identical indices, so we can take $R_{LT}=R_{sub}$. From Eqs. (4) and (5), the absorption coefficient of the LT-GaAs can be calculated as

$$\alpha_{LT} = \frac{\ln\left(\frac{I_{sub}}{I_{LT+sub}}\right)}{x_{LT}}. \tag{6}$$

The absorption spectrum of the LT-GaAs as derived from the transmission spectra of Figure 5.2.1 using Eq. (6) is shown in Figure 5.2.2. From this spectrum, a wide sub-bandgap absorption up to 1.5 μm wavelength was observed. The LT-GaAs still shows strong absorption (>1500 cm^{-1}) to beyond 1.5 μm wavelength making this a promising material for photodetectors. The inset in Figure 5.2.2 shows a wide absorption band below the bandgap energy and the expected sharp rise in absorption above the GaAs band edge (λ<900 nm). Manasreh [5] has observed the infrared absorption of two deep defects in LT-GaAs layers grown at 200 °C. One of these defects, of estimated concentration $\sim 3\times10^{18}/cm^3$, behaves like *EL2*, which is characterized as an As_{Ga}-related and photoquenchable defect; while the other, of estimated concentration $\sim 3\times10^{19}/cm^3$, resembles the photounquenchable isolated As_{Ga} antisite observed in neutron-irradiated GaAs materials. Both defects'

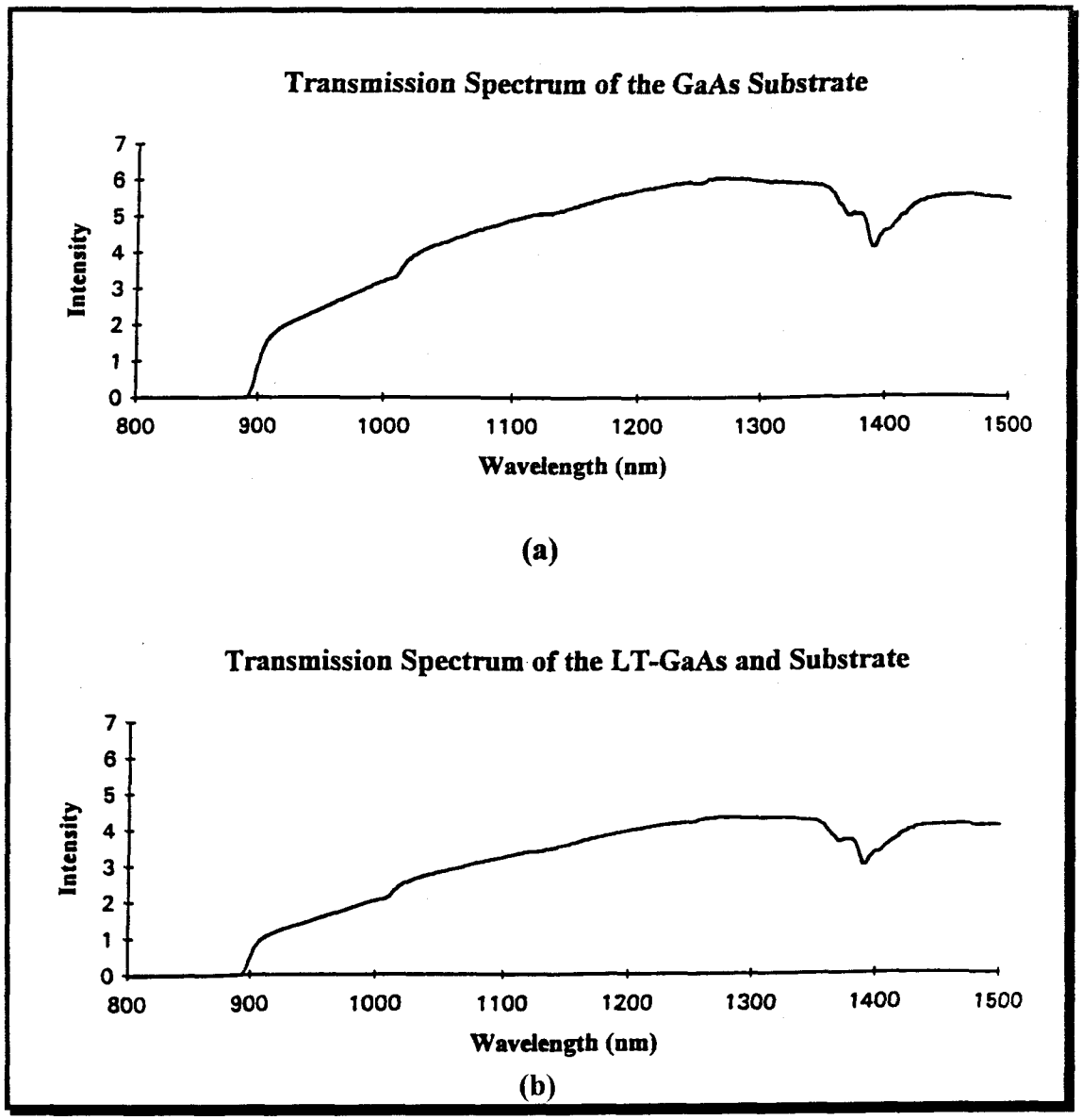

Figure 5.2.1 Transmission spectra using a 0.78 μm long pass filter. (a) Bare SI GaAs substrate, (b) 2 μm LT-GaAs MBE layer on SI GaAs substrate.

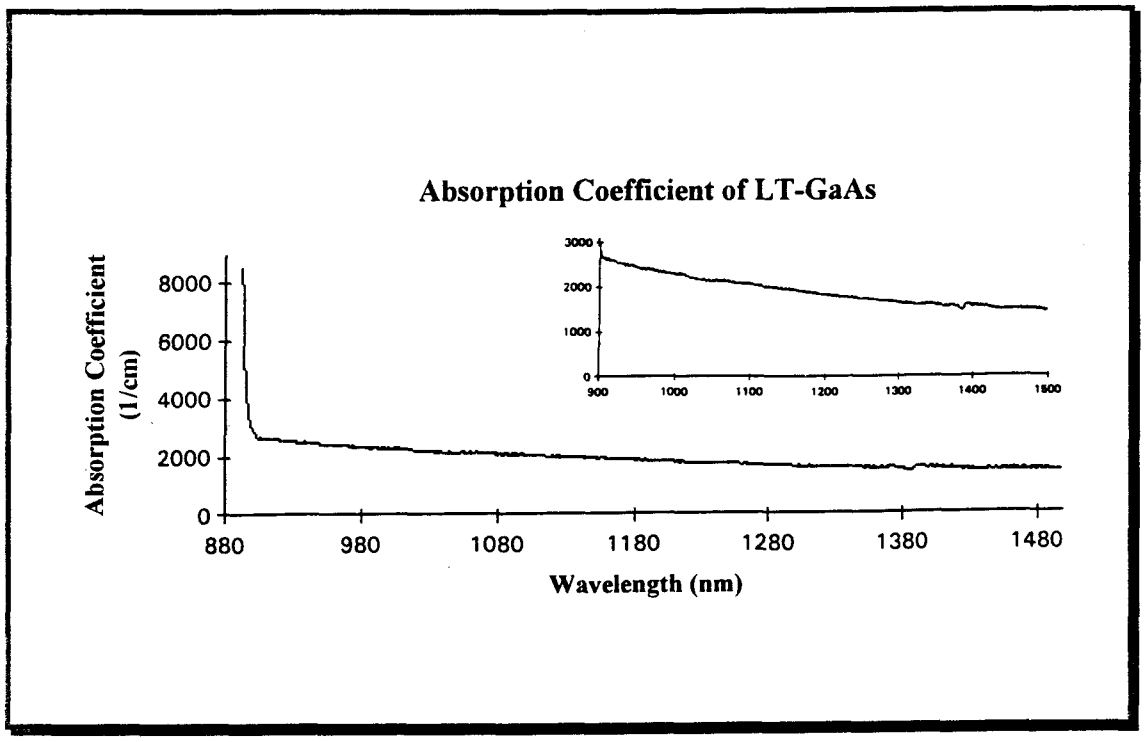

Figure 5.2.2 Infrared absorption spectrum of the 300 °C LT-GaAs.

concentrations are reduced by about an order of magnitude after thermal annealing at 600 °C for 10 minutes. The absorption due to *EL*2 after annealing was below the detection limit of the spectrophotometer. The remaining absorption spectrum in [5] is similar to the absorption spectrum we measured.

This sub-bandgap absorption can be explained using the following model [5]. The excess arsenic contained in the LT-GaAs has the form of precipitates. These arsenic precipitates act as buried Schottky barriers with spherical depletion regions and a barrier height of 0.7 eV. So the sub-bandgap absorption can occur from the bandgap of 1.43 eV (0.87 μm) to 0.7 eV (1.7 μm). GaAs grown by MBE at normal growth temperatures (around 600 °C) does not show significant absorption at wavelengths longer than 0.87 μm (corresponding to the GaAs bandgap). This result shows that the LT-GaAs is a useful material for long wavelength detector applications and could be easily integrated into a detector/amplifier circuit using GaAs amplifiers.

5.3 I-V Characteristics of the MSMPC and MODPC

Before the spectral and temporal response measurements, we performed an I-V measurement both in the dark and under He-Ne laser excitation for the MSMPC. The I-V characteristic curves are shown in Figure 5.3.1 for applied voltage from 0 to 10 volts. As expected, there is an additional current caused from the photoexcitation of electron-hole pairs in the semiconductor region between the contacts by the above-bandgap photon energies.

The I-V curves of the MODPC both in the dark and under microscope light excitation are shown in Figure 5.3.2 for applied voltage from 0 to 5 volts. Even under the microscope light excitation (which is much less intense than the He-Ne laser) and smaller bias voltages, the modulation-doped photodetector has larger current gain (~ 300) than the MSM photodetector. This larger signal is expected because electrons

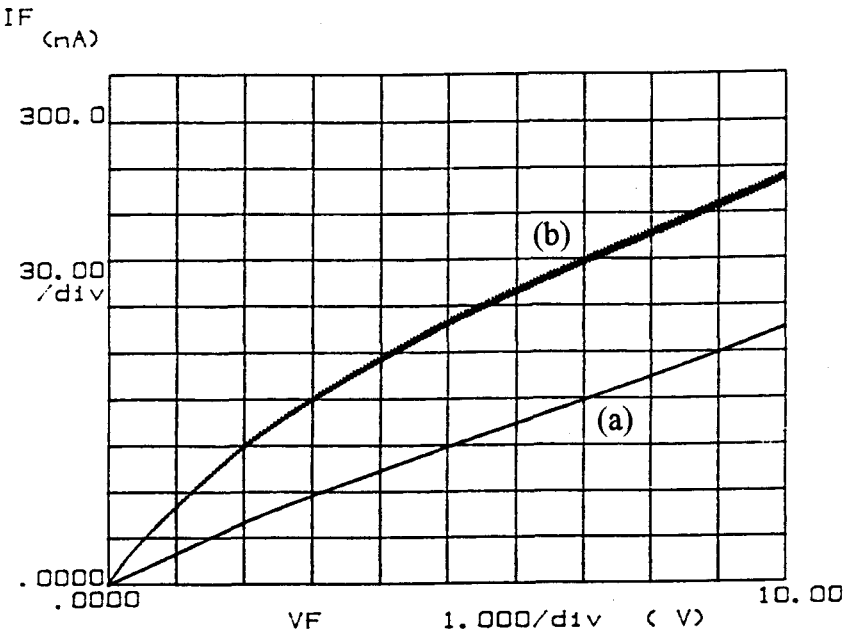

Figure 5.3.1 I-V characterization curves of the MSM photoconductor both (a) in the dark and (b) under He-Ne laser excitation.

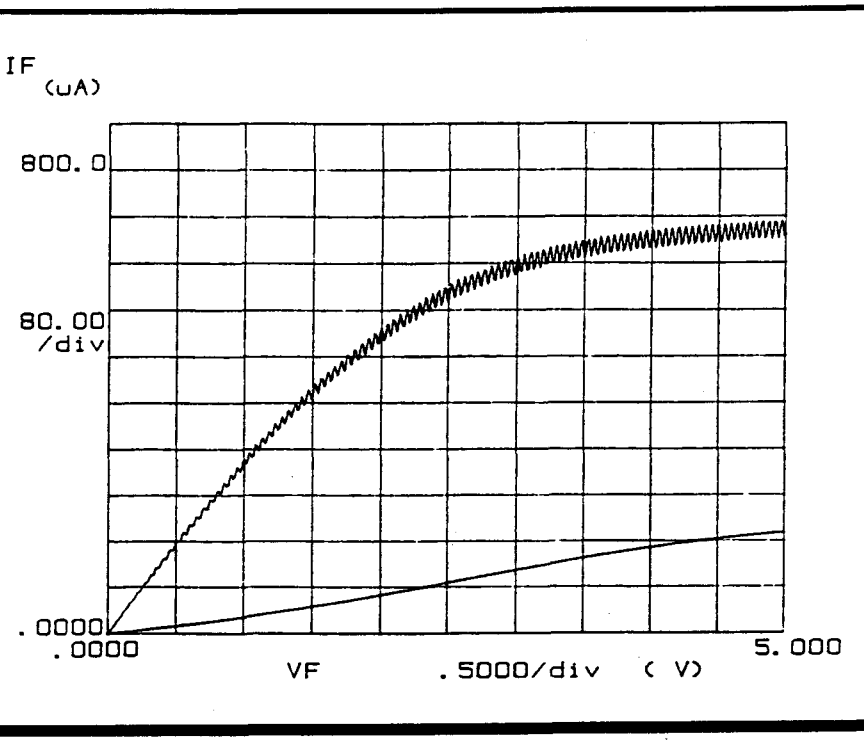

Figure 5.3.2 I-V characterization curves of the modulation-doped photoconductor both (a) in the dark and (b) under microscope light excitation .

generated in the LT-GaAs drift toward the interface and accumulate in the 2-D electron gas layer between the AlGaAs and the GaAs. At the same time, as a trade-off, the modulation-doped photodetector may have slower speed than the MSM photodetector due to the carrier separation by the built-in junction field and, therefore, a longer carrier lifetime due to recombination. The ripple on the illuminated I-V curves for LT-GaAs MSM photodetector is a real effect but is not yet understood. We did not see such ripple on similar MSM structures fabricated on SI GaAs or on regular 600 °C undoped GaAs MBE epilayers on SI substrates. We need to verify this again to make sure the ripple is not an instrument effect, but it could be a result of the LT defect structure and requires further study.

5.4 Spectral Response of the MSMPC and MODPC

The relative spectral response of the MSM photodetector is shown in Figure 5.4.1. The relative response, after correcting for the grating, lamp and Ge detector characteristics, decreases as the wavelength increases from 1000 nm to 1500 nm. This again can be explained by the Schottky barrier model. The excess arsenic precipitates act as buried Schottky barriers with a barrier height of 0.7 eV. The photoresponse is due to the internal photoemission of electrons from the precipitates into the GaAs. In this case, the observed spectral dependence is explained by the decreasing density of states in the conduction band as the photon energy decreases from 1.24 eV (100 nm) to 0.83 eV (1500 nm).

The spectral response of the MODPC was also measured. By using a germanium *p-i-n* photodetector to calibrate the light source and grating response, the relative spectral response was obtained and is shown in Figure 5.4.2 for different bias voltages. Starting at 715 nm, the cut-on wavelength of the filter, the spectral response shows a strong bandgap absorption and decreases to zero at the 870 nm bandgap

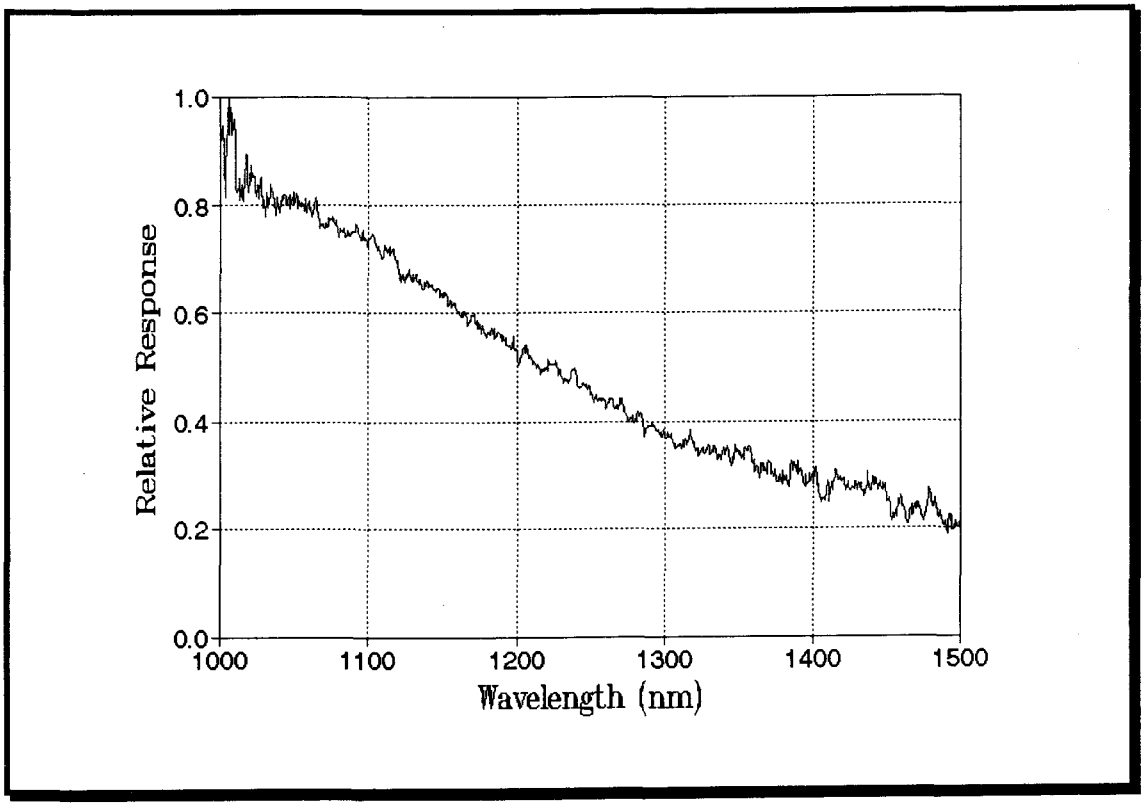

Figure 5.4.1 Relative spectral response of the MSM photoconductor.

wavelength. Additional sub-bandgap response is also observed. This response from 900-1300 nm is shown in more detail in Figure 5.4.3. As the bias voltage increases, the response also increases indicating an internal photocurrent gain in the device.

5.5 Temporal Response of the MSM Photodetector

Figures 5.5.1(a) and (b) show the photoresponse of the MSM photodetectors made on the LT-GaAs grown at 300 °C and 225 °C, respectively, to a train of 100 fs, 830 nm optical pulses from a Ti:sapphire laser. Both detectors have a much shorter decay time than previous GaAs MSM photodetectors made directly on SI GaAs [23]. The MSM photodetector made on the modified *p-i-n* diode material grown at 225 °C has a much shorter decay time than the 300 °C device. Even though the experimental setup was not optimized to minimize circuit ringing from pulse reflections, it is obvious that the 225 °C LT-GaAs material has a shorter lifetime than the 300 °C material and that it is shorter than 1 ns. With a better design of the 50 Ω transmission line mount and care in designing a 50 Ω match for the high impedance MSM photodetector, the University of Oregon system should allow us to measure lifetimes to the 25 ps limit of our sampling head. We have not directly compared the responsivity of the LT MSM devices to previous ones made on SI GaAs since devices of the same geometry were not available.

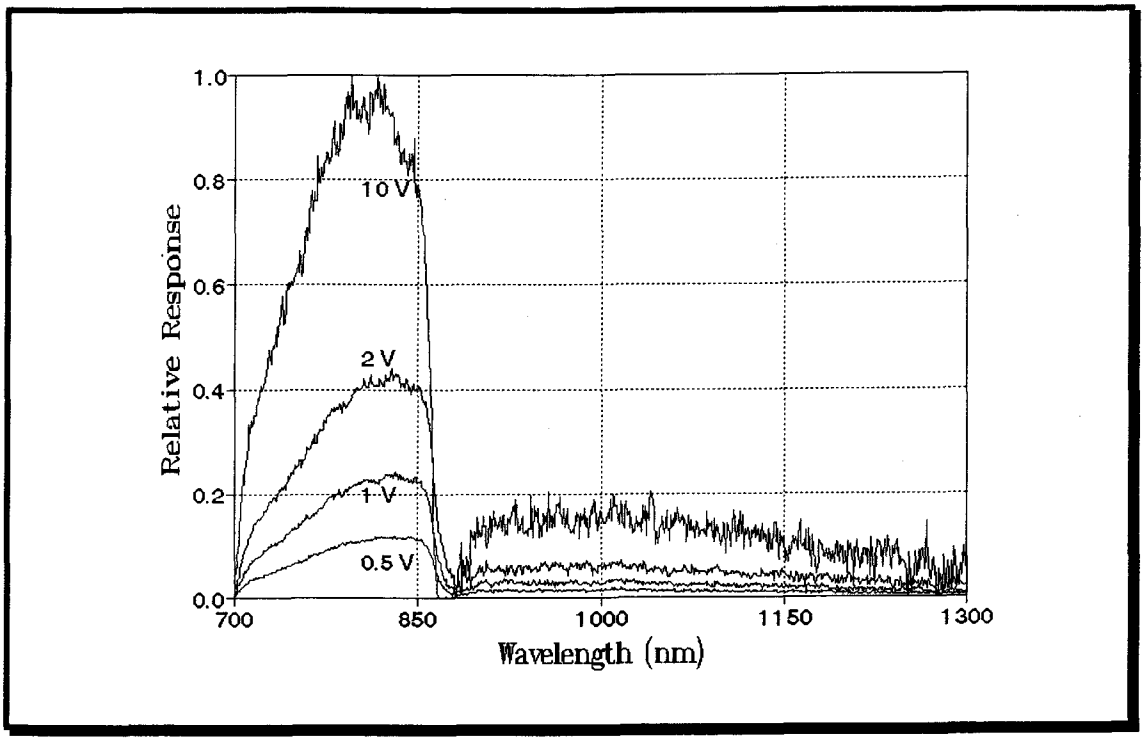

Figure 5.4.2 Relative spectral response of the modulation-doped photoconductor with different bias-voltages.

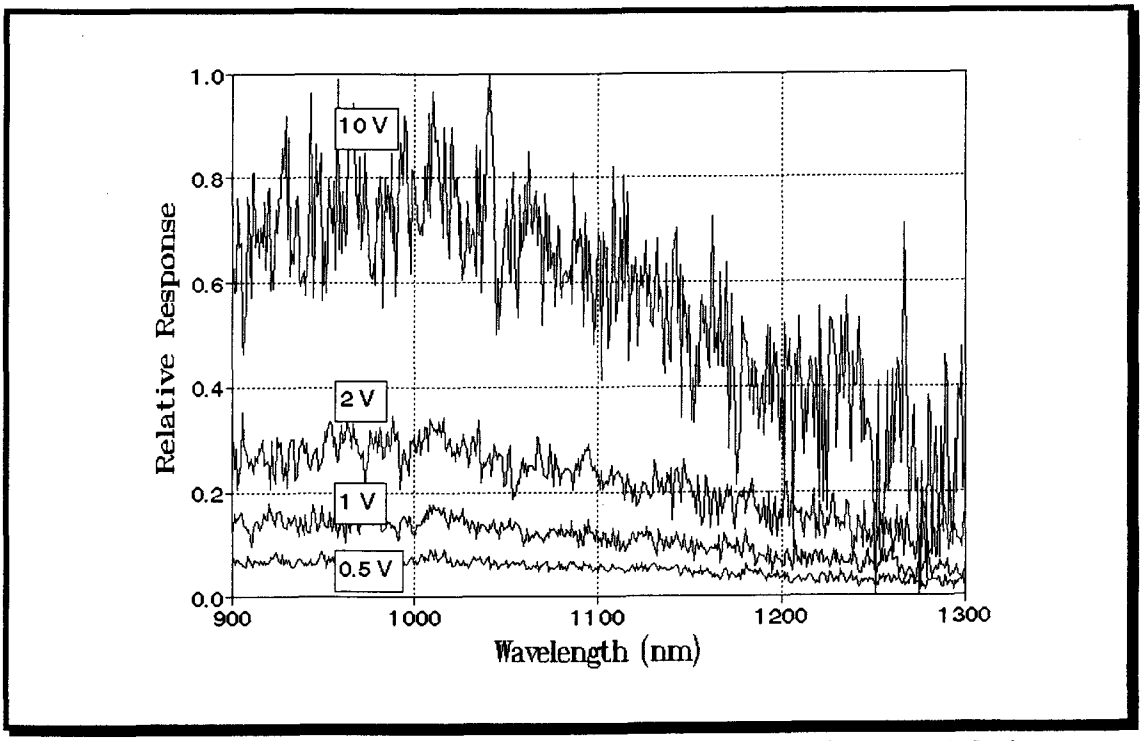

Figure 5.4.3 Relative sub-bandgap spectral response of the modulation-doped photoconductor with different bias-voltages.

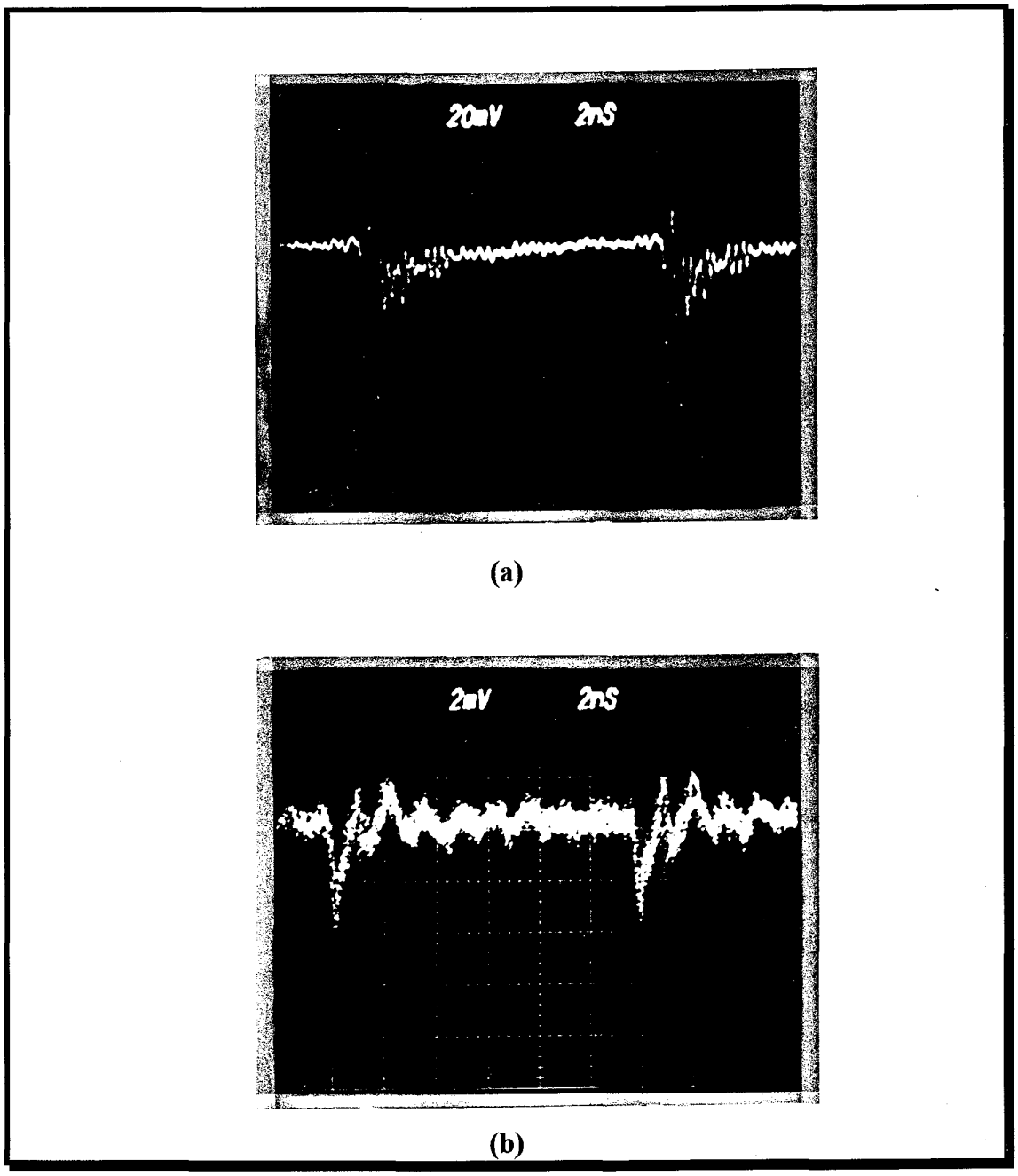

Figure 5.5.1 Response of the MSM photoconductor with the LT-GaAs grown at (a) 300 °C and (b) 225 °C to 100 fs pulses from a Ti:sapphire laser. A sampling scope with a 26 ps rise time was used. Horizontal scales are both 2 ns/div. Vertical scales are 20 mV/div in (a) and 2 mV/div in (b).

6. Conclusion and Suggestion for Future Research

In this thesis, the electrical and optical characteristics of MBE-grown LT-GaAs material have been investigated. Both MSM photoconductors and a new-type of modulation-doped LT-GaAs photoconductor have been fabricated and tested. The relative spectral responses of both kinds of photodetectors have been measured, and the temporal responses of the MSM photoconductors made on 225 °C and 300 °C LT-GaAs have been measured. Transport behavior of the LT-GaAs has been studied via the electrical testing of *p-i-n* diodes with the *i* layers grown at 225 °C, 300 °C, and 350 °C, respectively.

The major conclusions of this experimental investigation are summarized as following:

1. LT-GaAs has a wide sub-bandgap absorption, while normal MBE grown GaAs has only an *EL2* absorption shoulder in this energy range. From 900 nm to 1500 nm, the absorption coefficient of 300 °C LT-GaAs varies from 3000 /cm to 1500 /cm making this material useful for photodetectors in this sub-bandgap wavelength range.
2. Carrier lifetimes in LT-GaAs grown at 225 °C are probably ~6 ps, at 300 °C ~32 ps, and at 350 °C ~130 ps. These steady-state carrier lifetimes are about one magnitude order larger than the transient carrier lifetimes (sub-picosecond or picosecond), which are common in materials containing high concentrations of defects.
3. The sub-bandgap spectral responses of a LT-GaAs MSM photoconductor and a new modulation-doped photoconductor with LT-GaAs grown at 300 °C were measured. The modulation-doped photoconductor has much larger optical responsivity than the MSM photoconductor. Separation of electrons and holes by

the built-in junction field results in a longer carrier lifetime and, thus a gain of 300×.

4. The MSM photoconductor made on the SI LT-GaAs grown at 225 °C shows a faster optical impulse response than the one made on material grown at 300 °C. This indicates that bulk carrier lifetimes are shorter in the 225 °C material due to a larger number of defects and As precipitates.

The results of this work have demonstrated the difficulty of analyzing highly resistance material. Still, much has been learned and several useful photodetectors have been made. There are still many aspects of LT-GaAs to be investigated. Some of the measurements or devices to be made in the future are listed below.

1. Measure the low-temperature I-V characteristics of devices fabricated using LT-GaAs to study how the carrier transport properties change with temperature.
2. Fabricate *p-i-n* photodetectors using ring-shaped contact masks for use as 0.6 μm - 1.5 μm detectors.
3. Quantitatively determine the photoresponse of both the MSM photoconductor and the modulation-doped photoconductor and study these responses under different annealing conditions.
4. Use photolithographic techniques to deposit metal contacts and make etched Van der Pauw patterns on the SI LT-GaAs to directly measure the Hall mobility. Then study mobility as a function of temperature and annealing conditions.
5. Improve the optical impulse response measurements by designing an impedance-matched transmission line mount to avoid pulse ringing.
6. Explore a modulation-doped structure with a thin region of 600 °C GaAs at the 2-D gas layer to study the leakage behavior and the improvement in transport properties.

7. Bibliography

[1] S. M. Sze, *Physics of Semiconductor Devices, Second Edition*, John Wiley and Sons, New York, 1981.

[2] M. Kaminska, E. R. Weber, Z. Liliental-Weber, R. Leon, and Z. U. Rek, "Stoichiometry-related Defects in GaAs Grown by Molecular-beam Epitaxy at Low Temperatures", *J. Vac. Sci. Technol.*, volume B7, number 4, pp. 710-713, Jul/Aug 1989.

[3] A. C. Warren, J. M. Woodall, J. L. Freeouf, D. Grischkowsky, D. T. Mclnturff, M. R. Melloch, and N. Otsuka, "Arsenic Precipitates and the Semi-insulating Properties of GaAs Buffer Layers Grown by Low-temperature Molecular Beam Epitaxy", *Appl. Phys. Lett.*, volume 57, number 13, pp. 1331-1333, 24 September 1990.

[4] S. Gupta, J. Pamulapati, J. Chwalek, P. K. Bhattaacharya, and G. Mourou, "*Proceedings of Ultrafast phenomena VII*" (Springer, Berlin, 1990), p. 297.

[5] M. O. Manasreh, D. C. Look, K. R. Evans, and C. E. Stutz, "Infrared Absorption of Deep Defects in Molecular-Beam-Epitaxial GaAs Layers Grown at 200 °C: Observation of an *EL*2-like Defect", *Physical Review B*, volume 41, number 14, pp. 10272-10275, 1990.

[6] F. W. Smith, H. Q. Le, V. Diadiuk, M. A. Hollis, A. R. Calawa, S. Gupta, M. Frankel, D. R. Dykaar, G. A. Mourou, and T. Y. Hsiang, "Picosecond GaAs-based Photoconductive Optoelectronic Detectors", *Appl. Phys. Lett.*, volume 54, number 10, pp. 890-892, 6 March 1989.

[7] M. Klingenstein, J. Kuhl, R. Nötzel, K. Ploog, J. Rosenzweig, C. Moglestue, A. Hülsmann, and J. Schneider, "Ultrafast Metal-semiconductor-metal Photodiodes Fabricated on Low-temperature GaAs", *Appl. Phys. Lett.*, volume 60, number 5, pp. 627-629, 3 February 1992.

[8] F. W. Smith, A. R. Calawa, Chang-Lee Chen, M. J. Manfra, and L. J. Mahoney, "New MBE Buffer Used to Eliminate Backgating in GaAs MESFET's", *IEEE Electron Device Letters*, volume 9, number 2, pp. 77-80, February 1988.

[9] M. Kaminska, Z. Liliental-Weber, E. R. Weber, T. George, J. B. Kortright, F. W. Smith, B-Y. Tsaur, and A. R. Calawa, "Structural Properties of As-rich GaAs Grown by Molecular Beam Epitaxy at Low Temperatures", *Appl. Phys. Lett.*, volume 54, number 19, pp. 1881-1883, 8 May 1989.

[10] S. Gupta, M. Y. Frankel, J. A. Valdmanis, J. F. Whitaker, F. W. Smith, and A. R. Calawa, "Subpicosecond Carrier Lifetime in GaAs Grown by Molecular Beam Epitaxy at low Temperatures", *Appl. Phys. Lett.*, volume 59, number 25, pp. 3276-3278, 16 December 1991.

[11] H. M. van Driel, X. Q. Zhou, W. W. Rühle, J. Kuhl, and K. Ploog, "Photoluminescence from Hot Carriers in Low-temperature-grown Gallium Arsenide", *Appl. Phys. Lett.*, volume 60, number 18, pp. 2246-2248, 4 May 1992.

[12] X. Q. Zhou, H. M. van Driel, W. W. Rühle, Z. Gogolak, and K. Ploog, "Femtosecond Carrier Kinetics in Low-temperature-grown GaAs", *Appl. Phys. Lett.*, volume 61, number 25, pp. 3020-3022, 21 December 1992.

[13] T. Motet, J. Nees, S. Williamson, and G. Mourou, "1.4 ps Rise-time High-voltage Photoconductive Switching", *Appl. Phys. Lett.*, volume 59, number 12, pp. 1455-1457, 16 September 1991.

[14] A. C. Warren, J. H. Burroughes, J. M. Woodall, D. T. McInturff, R. T. Hodgson, and M. R. Melloch, "1.3-μm P-i-N Photodetector Using GaAs with As Precipitates (GaAs:As)", *IEEE Electron Device Letters*, volume 12, number 10, pp. 527-529, October 1991.

[15] D. T. McInturff, J. M. Woodall, A. C. Warren, N. Braslau, G. D. Pettit, P. D. Kirchner, and M. R. Melloch, "Photoemission Spectroscopy of GaAs:As Photodiodes", *Appl. Phys. Lett.*, volume 60, number 4, pp. 448-450, 27 January 1992.

[16] S. M. Sze, D. J. Coleman, Jr., and A. Loya, "Current Transport in Metal-Semiconductor-Metal (MSM) Structures", *Solid-State Electronics*, volume 14, pp. 1209-1218, 1971.

[17] V. Swaminathan, J. M. Freund, M. W. Focht, G. D. Guth, G. J. Przybylek, L. E. Smith, R. E. Leibenguth, and L. A. D'Asaro, "Ambipolar Lifetimes in GaAs/AlGaAs Self-Electro-Optic-Effect Devices", *Appl. Phys. Lett.*, volume 61, number 6, pp. 687-689, 10 August 1992.

[18] C. J. Sandroff, R. N. Nottenburg, J. C. Bischoff, and R. Bhat, "Dramatic Enhancement in the Gain of a GaAs/AlGaAs Heterostructure Bipolar Transistor by Surface Chemical Passivation", *Appl. Phys. Lett.*, volume 51, number 1, pp. 33-35, 6 July 1987.

[19] F. W. Smith, Ph.D. thesis, Massachusetts Institute of Technology, 1990.

[20] M. Zhuand H. Fritzsche, *Philos. Mag.*, volume B 53, number 41, 1986.

[21] R. S. Crandall and I. Balberg, "Mobility-lifetime Products in Hydrogenated Amorphous Silicon", *Appl. Phys. Lett.*, volume 58 number 5, pp. 508-510, 4 February 1991.

[22] E. S. Harmon, M. R. Melloch, J. M. Woodall, D. D. Nolte, N. Otsuka, and C. L. Chang, "Carrier Lifetime Versus Anneal in Low Temperature Growth GaAs", *Appl. Phys. Lett.*, volume 63 number 16, pp. 2248-2250, 18 October 1993.

[23] R. T. Kollipara, "Modeling and Testing of Semi-insulating Gallium Arsenide Interdigitated Photodetectors", PhD thesis, Oregon State University, 1991.

Appendices

Appendix A

p-i-n diode fabrication process steps.

1) Clean sample with trichloroethane (TCA), acetone, methanol and deionized water.
2) Mount sample upside down in evaporator centered over evaporation boats.
3) Pump down evaporator to 2E-6 torr and proceed with deposition of p-type ohmic contact metals, which is 100Å Ti, 150Å Au, 100Å Zn, and 1200Å Au.
4) Place sample on spinner.
5) Apply 1 to 2 drops of HMDS.
6) Start spinner and spin for 30 seconds, 6000 r.p.m.
7) Apply 1 to 2 drops of photoresist over sample.
8) Start spinner and spin for 30 seconds, 6000 r.p.m.
9) Softbake @85 °C for 25 minutes.
10) Place sample on wafer chuck of optical mask aligner and align the mask.
11) Exposure to ultraviolet light for 15 seconds and DI water rinse.
12) Immerse sample in developer for approximately 15 to 20 seconds.
13) Immerse sample in KI+I_2 Au etch solution for 20 seconds.
14) Rinse the sample in deionized water and blow dry with nitrogen gas.
15) Immerse sample in H_3PO_4:H_2O:H_2O_2=3:1:4 mesa etch solution for 20 seconds. The etch rate is about 5 μm/min.
16) Remove photoresist using acetone and blow dry.
17) Anneal sample @520 °C for 5 minutes in the forming gas.
18) Apply 1 to 2 drops of Na_2 S passivation solution over sample.
19) Start spinner and spin for 30 seconds, 6000 r.p.m.

Appendix B

MSM photoconductor fabrication process steps.

1) Clean sample with trichloroethane, acetone, methanol and deionized water.
2) Remove cap layer by immersing sample in $NH_4OH:H_2O_2:H_2O$=2:1:100 GaAs etch solution for 20 seconds.
3) Clean sample with trichloroethane (TCA), acetone, methanol and deionized water.
4) Place sample on spinner.
5) Apply 1 to 2 drops of HMDS.
6) Start spinner and spin for 30 seconds, 6000 r.p.m.
7) Apply 1 to 2 drops of photoresist over sample.
8) Start spinner and spin for 30 seconds, 6000 r.p.m.
9) Softbake @85 °C for 25 minutes.
10) Place sample on wafer chuck of optical mask aligner and align the mask.
11) Exposure to ultraviolet light for 15 seconds.
12) Immerse sample in chlorobenzene for 5 minutes.
13) Blow dry sample with nitrogen gas.
14) Immerse sample in developer for 1 minute and 20 seconds.
15) Rinse sample in deionized water and blow dry with nitrogen gas.
16) Prepare Veeco thermal evaporator.
17) Mount sample upside down in evaporator centered over evaporation boat.
18) Pump down evaporator to 2E-6 torr and proceed with deposition of Schottky contact, which is 1200 Å Au.
19) Spray acetone on sample till unwanted metal has lifted off.
20) Clean and blow dry sample.